1   # Correction of eIF2-dependent defects in brain protein synthesis,

2   # synaptic plasticity and memory in mouse models of Alzheimer's

3   # disease

4

5   Mauricio M. Oliveira[1,2], Mychael V. Lourenco[1], Francesco Longo[2], Nicole P. Kasica[3],

6   Wenzhong Yang[3], Gonzalo Ureta[4], Danielle D. P. Ferreira[5], Paulo H. J. Mendonça[1],

7   Sebastian Bernales[4], Tao Ma[3], Fernanda G. De Felice[1,6], Eric Klann[2,7,9], Sergio T.

8   Ferreira[1,8,9]

9

10   [1]Institute of Medical Biochemistry Leopoldo de Meis, Federal University of Rio de Janeiro,

11   Rio de Janeiro, RJ, Brazil

12   [2]Center for Neural Science, New York University, New York, NY, USA

13   [3]Department of Internal Medicine, Gerontology & Geriatric Medicine, Wake Forest

14   School of Medicine, Winston-Salem, NC, USA

15   [4]Fundación Ciencia & Vida, Santiago, Chile

16   [5]Institute of Biomedical Sciences, Federal University of Rio de Janeiro, Rio de Janeiro,

17   RJ, Brazil

18   [6]Centre for Neuroscience Studies and Department of Psychiatry, Queen's University,

19   Kingston, ON, Canada

20   [7]NYU Neuroscience Institute, New York University School of Medicine, New York, NY,

21   USA

1

22   [8]Institute of Biophysics Carlos Chagas Filho, Federal University of Rio de Janeiro, Rio de

23   Janeiro, RJ, Brazil

24   [9]Equal contribution

25

26

27   Corresponding authors: Sergio T. Ferreira (ferreira@bioqmed.ufrj.br); Eric Klann

28   (eklann@cns.nyu.edu)

29

30   Short title: ISRIB rescues memory in AD models

31   Keywords: Alzheimer's disease, integrated stress response, ISRIB, protein synthesis,

32   eIF2 alpha, mRNA translation.

33

34 **Abstract**

35 Neuronal protein synthesis is essential for long-term memory consolidation. Conversely,

36 dysregulation of protein synthesis has been implicated in a number of neurodegenerative

37 disorders, including Alzheimer's disease (AD). Several types of cellular stress trigger the

38 activation of protein kinases that converge on the phosphorylation of eukaryotic

39 translation initiation factor 2α (eIF2α-P). This leads to attenuation of cap-dependent

40 mRNA translation, a component of the integrated stress response (ISR). We show that

41 AD brains exhibit increased eIF2α-P and reduced eIF2B, key components of the eIF2

42 translation initiation complex. We further demonstrate that attenuating the ISR with the

43 small molecule compound ISRIB (ISR Inhibitor) rescues hippocampal protein synthesis

44 and corrects impaired synaptic plasticity and memory in mouse models of AD. Our

45 findings suggest that attenuating eIF2α-P-mediated translational inhibition may comprise

46 an effective approach to alleviate cognitive decline in AD.

47

48

49

50

51

52

53

54

55

56

Introduction

Alzheimer's disease (AD) is the most prevalent form of dementia, affecting more than 35 million people worldwide. Pathological hallmarks of AD include brain accumulation of the amyloid-β peptide (Aβ) and of neurofibrillary tangles composed of hyperphosphorylated tau protein, neuroinflammation, synapse failure/loss, and neurodegeneration, ultimately culminating in memory failure (*1*). Despite major progress in the elucidation of mechanisms of pathogenesis in recent years, AD is still a disease in urgent need of effective therapeutics capable of preventing and/or blocking progressive cognitive deterioration. Given the complex nature of AD, identification of molecular pathways and targets that effectively improve cognition has been challenging.

De novo protein synthesis plays a key role in synaptic plasticity and long-term memory consolidation (*2-7*). Initiation of cap-dependent mRNA translation involves the formation of a ternary complex comprising Met-tRNA, GTP and the eukaryotic initiation factor 2 (eIF2) complex. Activity of eIF2B, a guanine exchange factor (GEF), allows continuous ribosome assembly and mRNA translation (*8*). This step is tightly regulated by phosphorylation of eIF2 on its alpha subunit (eIF2α-P), which inhibits the GEF activity of eIF2B and attenuates global translation (*9, 10*).

Various cellular stress stimuli trigger activation of eIF2α kinases causing phosphorylation of eIF2α in a process termed the Integrated Stress Response (ISR). The ISR attenuates global cap-dependent protein synthesis while favoring the translation of a specific subset of mRNAs that help to restore cellular homeostasis (*11*). Increased translation of activating transcription factor 4 (ATF4, also known as CREB-2) is thought to be a central mediator of the ISR (*12*).

4

80   Mounting evidence implicates aberrant ISR and eIF2α-P in brain disorders,

81   including traumatic brain injury, prion disease, Down syndrome, and AD (*13-23*). ISR

82   markers are elevated in AD brains (*16, 24, 25*), as well as in the brains of mouse models

83   of AD (*15, 16, 26*). We previously demonstrated that either genetic ablation or inhibition

84   of eIF2α kinases rescues synapse function and memory defects in AD mouse models

85   (*15, 16*). We thus hypothesized that rescuing brain protein synthesis downstream of

86   eIF2α-P might be an attractive approach to correct cognitive impairment in AD.

87   Herein, we report that AD brains exhibit increased eIF2α-P levels accompanied by

88   reductions in eIF2B subunits. The ISR inhibitor, ISRIB, a small molecule compound that

89   stimulates eIF2B activity even in the presence of elevated eIF2α-P (*27-29*), rescued

90   reduced hippocampal protein synthesis and corrected impaired synaptic plasticity and

91   memory in AD model mice. Our findings suggest that targeting dysregulated brain

92   translational control by eIF2α may represent an effective approach to combat cognitive

93   failure in AD.

94

95   **Results**

96   *AD brains present increased eIF2α-P and reduced eIF2B subunit levels*

97   We first confirmed that cortical extracts from AD brains (see Supplementary Table

98   1 for demographics) displayed increased eIF2α-P (Fig. 1A), consistent with previous

99   findings (*16, 24*). No changes in total levels of the α and γ subunits of eIF2 were detected

100   (Fig. 1B,C). In contrast, both α (required for assembly) and ε (catalytic) subunits of eIF2B

101   were substantially reduced in AD (Fig. 1D,E). These results indicate that altered

102   translation initiation in AD brains is associated with ISR activation (as assessed by eIF2α-

5

103   P) and with reductions in eIF2B subunits. Because mRNA translation is central to long-

104   term memory consolidation, these findings suggest that rescuing brain eIF2-mediated

105   translation could be a target to treat memory failure in AD.

106

107   *ISRIB prevents eIF2α-P-induced impairment of long-term memory in mice*

108   We performed a proof-of-concept study to determine whether the ISR inhibitor,

109   ISRIB, could prevent memory impairment caused by brain accumulation of eIF2α-P.

110   ISRIB has been shown to bind to and stabilize the eIF2B complex in its active form,

111   thereby bypassing eIF2α-P to stimulate the free eIF2B pool (*29*). We first determined

112   whether systemic (i.p.) administration of ISRIB resulted in its accumulation in the mouse

113   brain. To this end, we administered ISRIB (0.25 mg/kg, i.p.) to mice for six consecutive

114   days and measured ISRIB concentrations in plasma and brain extracts by mass

115   spectrometry. Results showed that ISRIB could be detected in both plasma and brain at

116   4- and 24-hours following drug administration (Fig. 2A).

117   In another set of experiments, C57BL/6 mice were given daily injections of

118   salubrinal (1 mg/kg, i.p., for 5 consecutive days; Fig. 2B), an inhibitor of eIF2α

119   dephosphorylation). Long-term memory was then assessed using the Novel Object

120   Recognition (NOR) and Contextual Fear Conditioning (CFC) tasks. Treatment with

121   salubrinal impaired long-term memory in both NOR (Fig. 2C) and CFC (Fig. 2D) tests.

122   Systemic treatment of mice with ISRIB (0.25 mg/kg, i.p.) prevented memory impairments

123   induced by salubrinal in both NOR and CFC tests (Figs. 2C-D). ISRIB did not prevent the

124   increase in hippocampal eIF2α-P caused by salubrinal administration in mice (Fig. 2E)

125   but blocked the accumulation of ATF4, a central mediator of the ISR (Fig. 2F). These

126   findings are consistent with the notion that ISRIB acts downstream of eIF2α-P to restore

127   memory, and indicate that systemically administered ISRIB reaches the brain and

128   prevents memory impairments induced by the accumulation of eIF2α-P.

129

130   *ISRIB prevents eIF2α-P-mediated impairment in long-term memory in an acute model of*

131   *Alzheimer's disease*

132   We next asked whether ISRIB could counteract the activation of ISR and memory

133   deficits that are induced by amyloid-β oligomers (AβOs), toxins that accumulate in AD

134   brains and cause eIF2α-P-mediated synapse and memory failure (*1, 15, 30*). To

135   investigate this possibility, C57BL/6 mice received a single intracerebroventricular (i.c.v.)

136   infusion of AβOs (10 pmol, expressed as Aβ monomers; (*15, 31, 32*) followed by

137   administration of ISRIB (0.25 mg/kg, daily, i.p.) for the duration of the experiment (Fig.

138   3A). Because ISRIB has been reported to trigger pro-mnemonic effects (Sidrauski et al.,

139   2013), we did not inject ISRIB between training and test sessions of memory tasks. I.c.v.

140   infusion of AβOs induced hippocampal eIF2α-P (Fig. 3B) and increased ATF4 levels (Fig.

141   3C). Treatment with ISRIB counteracted the increase in hippocampal ATF4 protein levels

142   (but not mRNA; Figs. 3C and S1A) without affecting eIF2α-P levels (Fig. 3B).

143   We then hypothesized that ISRIB could correct translation defects induced by

144   AβOs. To test this hypothesis, we exposed ex vivo mouse hippocampal slices to AβOs (1

145   μM) in the absence or presence of ISRIB (0.2 μM) and assessed de novo protein

146   synthesis using SUnSET (*33*). We found that ISRIB prevented hippocampal translational

147   repression induced by AβOs (Fig. 3D). Similar results were obtained in primary neuronal

148   cultures using BONCAT (*34*) (Fig. 3E).

7

149   We further found that dendritic spine density was reduced in hippocampal CA1 in

150   mice that received an i.c.v. infusion of AβOs, and that systemic treatment with ISRIB

151   restored spine density in AβO-infused mice (Fig. 3F). i.c.v. infusion of AβOs caused

152   reductions in hippocampal synaptophysin, PSD-95 and BDNF, and treatment with ISRIB

153   had no effect on these proteins (Fig. S1B-E).

154   We next tested whether systemic treatment with ISRIB could prevent AβO-induced

155   cognitive impairment. We found that ISRIB prevented AβO-induced long-term memory

156   failure in both NOR (Fig. 3G) and CFC (Fig. 3H) tasks. Control measurements showed

157   no differences in locomotor or exploratory activities in mice that received an AβO infusion

158   and/or were treated with ISRIB (Fig. S2A-C), and no differences in the training phase in

159   either NOR or CFC tests (Fig. S2D,E). These findings indicate that ISRIB corrects AβO-

160   instigated eIF2α-P-dependent hippocampal translational repression, attenuates dendritic

161   spine loss, and rescues memory impairments in mice.

162

163   *ISRIB restores synapse function and memory in a transgenic mouse model of AD*

164   Next, we investigated whether ISR inhibition could reverse deficits in synaptic

165   plasticity and memory in 10-13 month-old APPswe/PS1ΔE9 mice, a transgenic mouse

166   model of AD characterized by age-dependent brain accumulation of Aβ (*35*). We initially

167   investigated the effect of ISRIB on long-term potentiation (LTP) in hippocampal slices

168   from APPswe/PS1ΔE9 mice. Whereas slices from APPswe/PS1ΔE9 mice failed to

169   maintain LTP at CA1 Schäffer collateral synapses following tetanic stimulation, treatment

170   with ISRIB restored LTP (Fig. 4A-B). We further found that ISRIB restored spine density

171   in pyramidal neurons from hippocampal CA1 region of APPswe/PS1ΔE9 (Fig. 4C).

172   To determine the effect of ISRIB on long-term spatial memory, we treated

173   APPswe/PS1ΔE9 mice (or WT littermates) with ISRIB (0.25 mg/kg, i.p.) daily for two

174   weeks before testing in the Morris water maze (MWM). This protocol was found to

175   alleviate the ISR in the hippocampus, as assessed by total levels of GADD34 (Fig. S3).

176   ISRIB improved learning in APPswe/PS1ΔE9 mice, as indicated by faster learning curves

177   compared to saline-treated APPswe/PS1ΔE9 mice (Fig. 4D), but did not improve memory

178   retention assessed in the MWM probe trial (Fig. 4E). However, ISRIB improved long-term

179   contextual memory of APPswe/PS1ΔE9 mice in the CFC test (Fig. 4F). Control

180   experiments showed that APPswe/PS1ΔE9 (or WT) mice treated with ISRIB had no

181   changes in locomotor or exploratory activities, and their weights were similar to control

182   animals (Fig. S4A-D). Results thus showed that treatment with ISRIB restores synaptic

183   plasticity and memory in APPswe/PS1ΔE9 mice.

184   We proceeded to determine whether treatment with ISRIB affected amyloid

185   deposition in the brains of APPswe/PS1ΔE9 mice. We found that ISRIB-treated

186   APPswe/PS1ΔE9 mice had reduced mean amyloid plaque size (Fig. 4G-I), but increased

187   plaque density in the hippocampal formation (Fig. 4J-K). Total $A\beta_{42}$ in the hippocampus

188   (Fig. 4L) and cortex (Fig. 4M) was unchanged by treatment. We hypothesized that the

189   reduced mean plaque size in APPswe/PS1ΔE9 mice treated with ISRIB could be due to

190   altered plaque phagocytosis by glial cells. APPswePS1ΔE9 mice exhibited increased

191   hippocampal immunoreactivities for Iba-1 (microglial marker) and GFAP (astrocytic

192   marker) compared to WT mice (Fig. S5). Treatment with ISRIB had no effect on either

193   Iba-1 (Fig. S5A-C) or GFAP (Fig. S5D-F) immunoreactivities in the hippocampi of

194   APPswe/PS1ΔE9 mice. Collectively, our findings indicate that ISRIB attenuates

9

195 translational repression, restores synaptic plasticity and memory independently of

196 amyloid burden in AD models.

197

198 **Discussion**

199 Activation of the ISR and attenuation of brain protein synthesis have been

200 implicated in memory deficits in AD (*15, 16, 24-26*) and in other neurodegenerative

201 disease (*13-23*), supporting the notion that correcting defective brain protein synthesis

202 might comprise an effective therapeutic target in AD. Because three out of four known

203 eIF2α kinases have been shown to play pathogenic roles in AD (*15, 16, 24, 25, 36, 37*),

204 identifying approaches that act downstream of eIF2α-P may comprise a more viable

205 strategy to alleviate cognitive impairment than simultaneously targeting individual

206 kinases. Here, we show that treatment with ISRIB, a small molecule compound that

207 targets ISR downstream of eIF2α, restores synaptic plasticity and long-term memory

208 defects in AD mouse models.

209 ISRIB has been shown to improve symptoms in rodent models of traumatic brain

210 injury, vanishing white matter disease, Down syndrome, SOD1-linked amyotrophic lateral

211 sclerosis (*38*), and prion disease (*18, 19, 22, 23, 39*). However, two previous studies have

212 reported no beneficial effects of ISRIB in AD model mice (*40*). We note that, in contrast

213 to our approach, the previous studies treated AD model mice with a single high-dose i.p.

214 injection of ISRIB (2.5-5 mg/kg). Briggs *et al*. (2017) further reported that prolonged

215 treatment of Tg2576 mice with 5 mg/kg ISRIB led to increased mortality (*40*), which differs

216 from our approach to treat mice with a low-dose of ISRIB (0.25 mg/kg) for several days,

217 which resulted in its detection in the plasma and brains of mice (as shown by LC-MS/MS).

10

218   Using this dosing regimen, we demonstrate beneficial effects of ISRIB on synapse

219   function and cognitive performance in two different mouse models of AD.

220   ISRIB was originally described as a memory-enhancing compound (*27*), and its

221   mechanism of action has now been extensively investigated. ISRIB binds to a regulatory

222   site and stabilizes eIF2B, stimulating its GEF activity independently of eIF2α-P (*29*), thus

223   favoring translational derepression. To the best of our knowledge, no off-target effect of

224   ISRIB has been reported.

225   Our ISRIB dosing regimen (low dose for several days) effectively restored eIF2α-

226   dependent translational control in AD mice, without noticeable biochemical or cognitive

227   effects in WT control mice. Differences between our results and those of Sidrauski *et al.*

228   (*27*) may be due to the fact that, in their case, a single and higher dose of ISRIB (5 mg/kg)

229   was administered within a critical window for memory consolidation, during which de novo

230   protein synthesis is essential for the persistence of newly formed memories (*41*). This is

231   in line with previous reports showing that ISRIB modifies the ISR under conditions of

232   increased eIF2α-P, but not under basal conditions (*42*), (*43*).

233   We found that ISRIB had a mild effect on aberrant hippocampal *Atf4* mRNA

234   expression in AβO-infused mice. Although not a canonical ISR event, increased *Atf4*

235   mRNA expression has been described as a consequence of ISR under some

236   circumstances (*44*) (*45*). Altogether, these data are consistent with the notion that ISRIB

237   acts downstream to eIF2α-P, restoring AD-linked molecular/cellular defects that are likely

238   driven by chronic low-grade activation of ISR.

239   Our findings indicate that ISRIB subtly alters amyloid pathology (reduced mean

240   plaque size; increased plaque density) without altering total Aβ_{42} load in the brains of

241   APPswe/PS1ΔE9 mice. One possibility is that the change in amyloid deposits may result

242   from overall resetting of proteostasis induced by ISRIB. Future studies aiming to identify

243   modifications induced by ISRIB treatment in the pool of mRNAs being translated may

244   reveal specific mechanisms of translational control of amyloid deposition.

245   We found no evidence of decreased microglial activation or astrocyte reactivity in

246   ISRIB-treated APPswe/PS1ΔE9 mice. Thus, it is conceivable that correction of eIF2-

247   dependent translational defects restores memory independently of key hallmarks of the

248   disease (total Aβ accumulation, glial reactivity) raising the prospect that boosting this

249   mechanism may improve cognitive function in patients already exhibiting noticeable

250   neuropathology.

251   ISRIB rescued impaired synaptic plasticity in the hippocampus of

252   APPSwe/PS1ΔE9 mice, in line with data showing that genetic correction of eIF2α-P levels

253   in neurons restores synaptic plasticity in APPswe/PS1ΔE9 mice (*16*). Moreover, we found

254   that ISRIB rescued reduced dendritic spine densities in both AβO-infused mice and

255   APPSwe/PS1ΔE9 mice. These observations suggest that the beneficial effects of ISRIB-

256   induced translational derepression on memory are linked to improved synapse stability

257   and function.

258   Our results further demonstrate a selective reduction in eIF2B subunits in AD

259   brains, consistent with a recent single-nucleus transcriptomic study showing that *EIF2B5*

260   expression is reduced in AD neurons (*46*). Although we cannot yet ascertain to what

261   extent the reduction in eIF2B subunits affects protein synthesis in AD, it is reasonable to

262   expect that GDP recycling and translation are impaired under those conditions. Thus,

263   ISRIB might still be effective by stimulating eIF2B assembly (*47*) and the GEF activity of

264   the remaining pool of eIF2B. This is consistent with our observation that acute treatment

265   with ISRIB rescued LTP in hippocampal slices from APPswe/PS1ΔE9 mice.

266   In conclusion, our findings establish eIF2α-P-dependent translational repression

267   as a potentially druggable target in AD, and open new avenues to investigate the

268   molecular mechanisms by which dysfunctional eIF2 signaling contributes to translational

269   repression in AD. Because the solubility of ISRIB might pose limits to its clinical

270   application, strategies aimed to attenuate the ISR or increase eIF2B activity by using

271   novel eIF2B activators (*22*) or repurposed compounds (*48*) may prove effective to target

272   brain protein synthesis and ward off cognitive decline in AD.

273

274   **Materials and Methods**

275   *Ethics.* All experiments with mice were carried out in accordance with the

276   "Principals of Laboratory Animal Care" (US National Institute of Health) guidelines and

277   performed under protocols approved and supervised by the Institutional Animal Care and

278   Use Committees of the Federal University of Rio de Janeiro (protocol number

279   IBQM039/16) and New York University (protocol number 09-1332).

280   *Postmortem human brain tissue.* Brain samples (prefrontal cortex) from non-

281   cognitively impaired and AD patients (defined by neuropathological criteria) were

282   obtained from the Emory University Brain Bank. Experimental procedures involving

283   human tissue were in compliance with the NYU Institutional Review Board (IRB).

284   Specimen information can be found in Supplementary Table 1. Post-mortem interval

285   (PMI) varied among donors, but average PMI was similar in AD versus control brains.

13

286   *Animals.* For the i.c.v. AβO-infusion model, we used three-month-old male and

287   female C57BL/6 mice, equally divided amongst experimental groups. To assess any

288   potential sex bias, we analyzed all groups divided by sex. Mice were obtained from the

289   animal facility at the Federal University of Rio de Janeiro and were maintained on a 12 h

290   light/dark cycle with food and water *ad libitum*, with 5 mice per cage. Transgenic

291   APPswePS1ΔE9 mice (B6/C3 background, JAX#34829) and WT littermates were

292   obtained from the New York University animal facility. Male and female mice (10-13

293   month-old) were used, and results were analyzed grouping both sexes together. Mice (4

294   to 5 per cage) were kept on a 12 h light/dark cycle with food and water *ad libitum*. For

295   every experiment, mice were pseudo-randomized into the different experimental groups,

296   and allocation of animals of the same cage in one experimental condition was avoided.

297   *Reagents.* ISRIB (> 98% purity) was from Sigma-Aldrich. Aβ$_{1-42}$ was purchased

298   from California Peptide. Culture media and IR dye-conjugated secondary antibodies were

299   from Li-Cor. Streptavidin-HRP, Streptavidin-AF594, ProLong anti-fade reagent, Tris-

300   glycine gels, and Aβ$_{42}$ ELISA kits were from Invitrogen. Anti-puromycin antibody (12D10)

301   was from EMD Millipore. Anti-ATF4, anti-GFAP, anti-eIF2Bα, anti-eIF2Bε, anti-eIF2γ,

302   anti-β-actin antibodies, and BDNF ELISA kits were from Abcam. Anti-eIF2α-P(Ser51),

303   anti-eIF2α and anti-β-tubulin were from Cell Signaling Technology. 6E10 antibody was

304   from Enzo Life Sciences. Biotin-conjugated anti-Iba1 was from Wako Fujifilm. BCA

305   protein assay kit was from Thermo Fisher. Laemmli Buffer (4x) was from Bio-Rad. Alkyne-

306   conjugated biotin and Protein Reaction Buffer kit were from Click Chemistry Tools.

307   *ISRIB determination by LC-MS/MS.* Analysis of plasma and brain samples were

308   conducted on a QTRAP 4500 triple quadrupole mass spectrometer (Applied Biosystems

14

309 SCIEX) in the positive ion mode and interfaced with an Ekspert ultraLC 100-XL UHPLC

310 System (Eksigent). Calibration standards (0.003 to 10 µM ISRIB) and quality controls

311 (0.02, 0.2 and 2.0 µM) were prepared in naïve mouse plasma in parallel with mouse

312 plasma study samples (60 µL) by precipitation with three volumes of ice-cold internal

313 standard solution (acetonitrile containing 20 µM theophylline). Precipitated samples were

314 centrifuged at 6,100 x g for 30 min at 4 °C. Following centrifugation, an aliquot of each

315 supernatant was transferred to an autosampler vial and diluted with two volumes of

316 aqueous mobile phase (0.2% formic acid in water). Samples were injected onto a reverse

317 phase analytical column (YMC Triart C18; 2.0 x 50 mm; 1.9 µm; YMC CO) and eluted

318 with a gradient of 0.2% formic acid in acetonitrile. ISRIB and internal standard were

319 monitored by a multiple reaction monitoring (MRM) experiment using Analyst software

320 (v1.6.2, Applied Biosystems SCIEX). Quantitation was conducted using MultiQuant

321 software (v2.1, Applied Biosystems SCIEX) and the resulting calibration curve was fitted

322 by linear regression and 1/x weighting. The lower limit of quantitation (LLOQ) was 0.003

323 µM.

324   *Preparation and characterization of amyloid-β oligomers (AβOs).* AβOs were

325 prepared as described (*49*), and each and every preparation was characterized by size-

326 exclusion chromatography (SEC-HPLC), as previously described (*15, 31, 32, 50*). AβO

327 preparations were kept at 4 °C and used within 48 h of preparation.

328   *Primary neuronal cultures.* Pregnant mice were euthanized on the 19th day of

329 gestation, and embryonic brains were collected. Hippocampi and cortices were dissected

330 and homogenized in HBSS containing 0.37% D-glucose. Tissue lumps were removed

331 with a cell restrainer, the cell suspension was centrifuged at 1,500 rpm/5 min and the

15

332   pellet was re-suspended in DMEM containing 10% fetal bovine serum (FBS). Cell number

333   was estimated using a Neubauer chamber. Cells were plated in (poly-L-lysine + laminin)-

334   coated plates and incubated at 37 °C in a 5% CO_2 atmosphere for 1h. DMEM was then

335   replaced by Neurobasal medium supplemented with Pen/Strep, Glutamax and 2% B27.

336   Cultured primary neurons were maintained at 37 °C in a 5% CO_2 atmosphere for 10 days

337   for maturation before experiments. Cells were treated on DIV 12-13 with 0.5 µM AβOs (or

338   vehicle) in the absence of presence of 0.2 µM ISRIB, prepared as previously described

339   (*19*).

340   *Western blotting.* Human and mouse brain tissue samples were homogenized by

341   sonication in RIPA buffer + Halt Protease/phosphatase inhibitor cocktail. Homogenates

342   were centrifuged at 10,000 x *g*/10 min at 4 °C, and the supernatant was harvested for

343   Western blot analysis. Protein concentration was determined by BCA, following

344   manufacturer's instructions. Protein samples were prepared to a final concentration of 5

345   µg/µl in 4x Laemmli buffer (Bio-Rad) containing 25 mM DTT. Samples were boiled for 3

346   min and 50 µg total protein were loaded per lane and resolved in 4-12% SDS-containing

347   Tris-glycine gels. Proteins then were transferred to PVDF or nitrocellulose membranes.

348   Primary antibodies were used in the following dilutions: 1:10,000 anti-β-actin; 1:2,500

349   anti-puromycin; 1:1,000 anti-ATF4, anti-eIF2α, anti-eIF2α-P; 1:500 anti-eIF2Bε, anti-

350   eIF2Bα, anti-eIF2γ. Secondary antibodies, either IR dye-conjugated (Li-Cor) or

351   horseradish peroxidase (HRP)-conjugated, were used at 1:10,000 dilution. ECL plus was

352   used to develop HRP-labeled blots.

353   *RT-PCR.* Total RNA was extracted from cultures using the SV Total RNA Isolation

354   System (Promega), following manufacturer's instructions. RNA concentration and purity

355   were determined by absorption at 260 nm and 280 nm. For quantitative real-time reverse

356   transcription PCR (qRT–PCR), 1 µg of total RNA was used for complementary DNA

357   (cDNA) synthesis using the High Capacity cDNA Reverse Transcription kit (ThermoFisher

358   Scientific). Quantitative expression analysis of targets was performed on a 7500 Fast

359   Real-Time PCR system (ThermoFisher Scientific) with the Power SYBR Green PCR

360   Master Mix. β-Actin (actb) was used as an endogenous reference gene for data

361   normalization. qRT–PCR was performed in 15 µl reaction volumes. Primer sequences

362   used for Atf4 and Actb amplification were: Fwd Atf4 – CCACCATGGCGTATTAGAGG;

363   Rev   ATF4   –   CTGGATTCGAGGAATGTGCT;   Fwd   Actb   –

364   TGTGACGTTGACATCCGTAAA; and Rev Actb – GTACTTGCGCTCAGGAGGAG. Cycle

365   threshold (CT) values were used to calculate fold-changes in gene expression using the

366    $2^{-\Delta\Delta Ct}$ method (51).

367   *ELISA*. Tissue samples were homogenized in 100 mM Tris, 150 mM NaCl, 1 mM

368   EGTA, 1 mM EDTA, and 1% Triton X-100, supplemented with protease and phosphatase

369   inhibitor cocktail (ThermoFisher). ELISAs for BDNF and $A\beta_{42}$ were run following

370   manufacturer's instructions.

371   *BONCAT*. Bio-Orthogonal Noncanonical Amino Acid Tagging (BONCAT) was

372   utilized for de novo protein synthesis assessment (52). Primary neuronal cultures had

373   their medium replaced by methionine-free RPMI supplemented with 2% B27, 1%

374   Glutamax and 0.25% glucose. Cells were incubated for 30 min to allow for methionine

375   starvation and azidohomoalanine (AHA), a methionine analog azide, was added at 1 mM

376   final concentration to label newly synthesized proteins. $A\beta Os$ (0.5 µM) and/or ISRIB (0.2

377   µM) were added, and cells were incubated for 2 h at 37 ºC. Cellular content was harvested

17

378   using RIPA buffer (Pierce) supplemented with Halt Protease/Phosphatase inhibitor

379   cocktail. Protein levels were determined using the BCA method (Thermo Pierce). AHA-

380   conjugated proteins were biotinylated using the Protein Reaction Buffer kit (Thermo

381   Fisher), following manufacturer's instructions. Newly synthesized proteins were

382   precipitated using streptavidin-conjugated resin and were detected by Western blotting

383   using streptavidin-conjugated HRP (1:2,000).

384   *SUnSET*. Hippocampal slices were prepared as previously described (*16*). Briefly,

385   400 μm hippocampal slices were obtained using a chopper, and recovered in artificial

386   cerebrospinal fluid (aCSF) for 1h. Slices were then exposed to 1 μM AβOs (or vehicle) in

387   the absence or presence of 0.2 μM ISRIB for 3h. Puromycin was added to the media to

388   a final concentration of 5 μg/ml during the last hour of the experiment. After incubation,

389   slices were flash frozen and processed for Western blotting. Puromycin incorporation was

390   quantitated as a measure of newly synthesized proteins. The representative image shown

391   in Figure 3J had its brightness level linearly increased solely for visualization purposes,

392   but quantification of incorporated puromycin was performed in raw images without any

393   manipulation.

394   *Animal treatments*. Intracerebroventricular (i.c.v.) infusions of AβOs were

395   performed as described previously (*15, 31, 32, 53*). Mice were anesthetized briefly with

396   2% isoflurane and AβOs were injected 1 mm to the right of the midline point equidistant

397   of each eye and 1 mm posterior to a line drawn through the anterior base of the eyes.

398   Mice were then placed back in their cages.

399   Mice were injected daily intraperitoneally with 0.25 mg/kg ISRIB or vehicle (200 μL

400   per injection). Treatment regimen is described in each section of "Results" and followed

18

401   a protocol previously established in literature, known to have a beneficial effect in a

402   murine model of prion disease (*18*). Using this protocol, Halliday and co-workers (2015)

403   showed that substantial amounts of ISRIB reached the brain and persisted for at least

404   24h. For salubrinal experiments, mice were concomitantly injected daily with ISRIB (0.25

405   mg/kg) and salubrinal (1 mg/kg). Results obtained in this study were used as a template

406   for subsequent studies using AD mouse models.

407   *Behavioral analyses.* Long-term memory was assessed using the Novel Object

408   Recognition (NOR), Contextual Fear Conditioning (CFC), and Morris water maze (MWM)

409   tests, as described below. Locomotor activity was assessed in an Open Field Arena

410   (OFA). In all behavioral experiments, the experimenter was blinded to the groups tested.

411   Animals that had biased exploration during training in the NOR (100% exploration of a

412   specific object during training phase) were excluded from analysis. In the MWM, mice

413   that did not swim during trials were excluded from both the learning analysis and the

414   probe trial. Finally, in the CFC task, mice with unaltered behavior after being shocked

415   were excluded from the analysis.

416   *Novel Object Recognition.* Tests were carried out using a NOR box (30 x 30 x 50

417   cm). In the training phase, mice were exposed to two identical objects, which they were

418   allowed to freely explore for 5 minutes. Time spent exploring each object was recorded

419   and twenty-four hours later, in the test phase, one of the objects was replaced by a novel

420   object. Mice again were exposed to the objects for 5 minutes, and the total exploration

421   time of both old (familiar) and new (novel) objects were determined. Discrimination index

422   was determined by: $(T_{novel} - T_{familiar}) / (T_{novel} + T_{familiar})$. After the task was completed, mice

423   were placed in a different arena for 5 minutes, where total distance, average velocity and

19

424   total time spent at the periphery were recorded and determined using ANY-Maze software

425   (Stoelting Co.).

426   *Contextual Fear Conditioning.* To assess contextual fear memory, a two-phase

427   protocol was used, as described (*15, 54*) with minor modifications. In the training phase,

428   mice were presented to the conditioning cage (40 x 25 x 30 cm), which they were allowed

429   to freely explore for 2 minutes followed by application of a single foot shock (0.35 mA) for

430   2 s. Mice were kept for another 30 s in the cage and removed. On the next day, mice

431   were presented to the same cage for 5 minutes without receiving a foot shock. Freezing

432   behavior was recorded automatically using the Freezing software (Panlab) and was used

433   as a memory index. For APPSwe/PS1∆E9 mice, due to the extensive memory impairment

434   in these mice, protocol included 2 min of free exploration, followed by two foot shocks

435   (0.8 mA), 2 s each, spaced by 30 s. Mice were then kept for another 2 min in the cage

436   and removed.

437   *Morris water maze.* The Water Maze test was carried out as previously described

438   (*16, 55*). Briefly, 3 training sessions per day were carried out for 5 days, except in the first

439   day, when mice were trained in 4 sessions. Time to reach the platform was recorded as

440   a measure of learning capacity. Average velocity and total distance traveled in the pool

441   were recorded as control locomotor parameters. Probe trials were performed for 1 minute

442   24 h after the last training session. Time spent in the target quadrant was recorded as a

443   memory output. Recording was performed using Ethovision software.

444   *Open Field Arena.* Locomotor activity in APPswePS1∆E9 mice was assessed

445   using the OFA (Med Associates Inc). Mice were allowed to freely explore the box for 15

446   min, during which their movement was recorded using Activity MDB software (Med

20

447 Associates Inc). Total distance traveled, average velocity and total time spent at the

448 periphery were recorded.

449   *Golgi staining.* Mice were euthanized and whole brains were carefully harvested,

450 rinsed in PBS and prepared for Golgi staining using the FD Rapid Golgi Kit (FD

451 Neurotechnologies) following manufacturer's instructions. Briefly, brains were immersed

452 in a mixture containing solutions A and B (1:1) for 14 days protected from light, with gentle

453 swirling twice a week. Brains were then incubated in solution C for 72 hours before

454 sectioning. After staining, brains were sliced on a Leica Vibratome in 200 µm-thick

455 sections and developed for 5 minutes in solutions D and E, followed by dehydration.

456 Slices were mounted on gelatin-coated slides and imaged on a Nikon Eclipse TE2000-U

457 microscope under bright field illumination. For dendritic spine quantification, 3 dendrite

458 segments of 10-20 µm that were at least 50 µm from the cell soma were selected per

459 neuron. Five neurons were analyzed per brain. Total dendritic spines in each segment

460 were counted and normalized by total length of the dendritic segment. For image analysis,

461 the experimenter was blinded to the conditions analyzed. For visualization purposes,

462 representative images shown in Figure 3E had their brightness and contrast linearly

463 altered, but spine counting was performed in the absence of any image manipulation.

464   *Electrophysiology.* Acute 400 µm transverse hippocampal slices from WT or

465 APPswe/PS1∆E9 mice were prepared using a Leica VT1200S vibratome as described

466 previously (*56*). Slices were maintained at room temperature for at least 2 h in artificial

467 cerebrospinal fluid (aCSF) containing (in mM) 118 NaCl, 3.5 KCl, 2.5 $CaCl_2$, 1.3 $MgSO_4$,

468 1.25 NaH_2PO_4, 5.0 $NaHCO_3$ and 15 glucose, bubbled with 95% O_2 / 5% CO_2. For

469 electrophysiology, monophasic, constant-current stimuli (100 µs) were delivered with a

21

470   bipolar silver electrode placed in the stratum radiatum of area CA3. Field excitatory

471   postsynaptic potentials (fEPSPs) were recorded using a glass microelectrode from the

472   stratum radiatum of area CA1. Late-LTP (L-LTP) was induced using high-frequency

473   stimulation (HFS) consisting of two 1-sec 100 Hz trains separated by 60 sec, each

474   delivered at 70-80% of the intensity that evoked spiked fEPSPs. Slices were perfused

475   with ISRIB (0.2 µM in ACSF) or vehicle during the whole recording process.

476   *Immunohistochemistry*. WT and APPSwe/PS1∆E9 treated with ISRIB (as

477   described above) were anesthetized with a ketamine/xylazine mixture. Mice were first

478   perfused with PBS for 45 seconds, and then with 4% PFA for 90 seconds. Brains were

479   carefully removed from the skull and post-fixed in 4% PFA for 48h at 4 °C, under agitation.

480   Brains were blocked on 3% agarose and sectioned using a VT1200 S vibratome (Leica

481   Biosystems), to 40 µm sections. Sections were kept at 4 °C until use. For Aβ (6E10), Iba1

482   and GFAP staining, free-floating sections were initially permeabilized using 0.5% Triton

483   X-100 solution for 15 min. Sections were then blocked for 1h with 5% NGS, and incubated

484   overnight with 6E10 (mouse, 1:200) and anti-GFAP (chicken, 1:1000) solution. Sections

485   were washed 3 times using 0.1% Triton X-100 and incubated with anti-rabbit and anti-

486   chicken secondary antibodies (1:500) for 90 min. Sections were again washed 3 times

487   with 0.1% Triton X-100 and subsequently incubated overnight with biotin-conjugated anti-

488   Iba1 (rabbit, 1:500). Sections were washed 3 times using 0.1% Triton X-100 and

489   incubated with Alexa Fluor 594-conjugated streptavidin (1:500) for 90 min. Sections were

490   washed 3 times with 0.1% Triton X-100 and mounted using Prolong with DAPI. Imaging

491   was performed on a Leica SP8 confocal microscope. Images were acquired and analyzed

492   using identical parameters across the experiment. Total fluorescence was determined by

22

493 generating a mask in Fiji. The mask was used to determine the threshold separating

494 signal and noise. Total pixel intensity (determined by the "Raw Integrated Density"

495 variable) was then obtained using the whole image as region of interest (ROI). For glial

496 content surrounding plaques, 20X magnification images were used. A region containing

497 the plaque and an ~30 µm radius surrounding area was used as ROI. Total Iba1 or GFAP

498 fluorescence were determined as above. For image analysis, the experimenter was

499 blinded to the conditions.

500   *Statistical analysis*. Pilot experiments were performed to allow calculations of

501 sample and effect sizes by power analysis. G Power software (Düsseldorf University) was

502 used for power analysis calculations after determination of the statistical analysis that

503 would be used to analyze each experiment. Statistical analyses were performed using

504 GraphPad Prism 6 software. Differences between two independent groups were analyzed

505 using Student's t-test. When three or more independent experimental groups were

506 compared, ANOVA was used, followed by appropriate *post-hoc* tests, as stated in "Figure

507 Legends" and in Supplemental Table 2.

508

509 **Supplementary Materials**

510

511 **Figure S1.** ISRIB does not attenuate the increase in hippocampal Atf4 mRNA, or the

512 reductions in BDNF, PSD-95 and synaptophysin induced by AβOs in mice.

513 **Figure S2.** ISRIB does not alter locomotor activities.

514 **Figure S3.** ISRIB restores GADD34 levels in the hippocampus of APPSwe/PS1∆E9 mice.

515 **Figure S4.** Locomotor/exploratory activities and body weight of APPswe/PS1ΔE9 are not

516 altered by ISRIB treatment.

517 **Figure S5.** Gliosis in APPSwe/PS1ΔE9 hippocampus (dentate gyrus/stratum lacunosum

518 moleculare) is unaffected by ISRIB treatment.

519 **Fig S6.** Full Western blots used in the current study.

520 **Supplementary Table 1.** Demographics of control and AD brains.

521

References

523 1. D. J. Selkoe, J. Hardy, The amyloid hypothesis of Alzheimer's disease at 25 years. *EMBO*
524   *Mol Med* **8**, 595-608 (2016); published online EpubJun (10.15252/emmm.201606210).
525 2. L. B. Flexner, J. B. Flexner, R. B. Roberts, G. Delahaba, Loss of Recent Memory in Mice
526   as Related to Regional Inhibition of Cerebral Protein Synthesis. *Proc Natl Acad Sci U S A*
527   **52**, 1165-1169 (1964); published online EpubNov (10.1073/pnas.52.5.1165).
528 3. M. Costa-Mattioli, D. Gobert, H. Harding, B. Herdy, M. Azzi, M. Bruno, M. Bidinosti, C.
529   Ben Mamou, E. Marcinkiewicz, M. Yoshida, H. Imataka, A. C. Cuello, N. Seidah, W.
530   Sossin, J. C. Lacaille, D. Ron, K. Nader, N. Sonenberg, Translational control of
531   hippocampal synaptic plasticity and memory by the eIF2alpha kinase GCN2. *Nature* **436**,
532   1166-1173 (2005); published online EpubAug 25 (10.1038/nature03897).
533 4. M. Costa-Mattioli, D. Gobert, E. Stern, K. Gamache, R. Colina, C. Cuello, W. Sossin, R.
534   Kaufman, J. Pelletier, K. Rosenblum, K. Krnjevic, J. C. Lacaille, K. Nader, N. Sonenberg,
535   eIF2alpha phosphorylation bidirectionally regulates the switch from short- to long-term
536   synaptic plasticity and memory. *Cell* **129**, 195-206 (2007); published online EpubApr 6
537   (10.1016/j.cell.2007.01.050).
538 5. M. A. Trinh, E. Klann, Translational control by eIF2alpha kinases in long-lasting synaptic
539   plasticity and long-term memory. *Neurobiol Learn Mem* **105**, 93-99 (2013); published
540   online EpubOct (10.1016/j.nlm.2013.04.013).
541 6. G. V. Di Prisco, W. Huang, S. A. Buffington, C. C. Hsu, P. E. Bonnen, A. N. Placzek, C.
542   Sidrauski, K. Krnjevic, R. J. Kaufman, P. Walter, M. Costa-Mattioli, Translational control
543   of mGluR-dependent long-term depression and object-place learning by eIF2alpha. *Nat*
544   *Neurosci* **17**, 1073-1082 (2014); published online EpubAug (10.1038/nn.3754).
545 7. A. N. Placzek, G. V. Prisco, S. Khatiwada, M. Sgritta, W. Huang, K. Krnjevic, R. J.
546   Kaufman, J. A. Dani, P. Walter, M. Costa-Mattioli, eIF2alpha-mediated translational
547   control regulates the persistence of cocaine-induced LTP in midbrain dopamine neurons.
548   *Elife* **5**, (2016); published online EpubDec 13 (10.7554/eLife.17517).
549 8. R. J. Jackson, C. U. Hellen, T. V. Pestova, The mechanism of eukaryotic translation
550   initiation and principles of its regulation. *Nat Rev Mol Cell Biol* **11**, 113-127 (2010);
551   published online EpubFeb (10.1038/nrm2838).

552   9.   G. D. Pavitt, Regulation of translation initiation factor eIF2B at the hub of the integrated
553   stress response. *Wiley Interdiscip Rev RNA* **9**, e1491 (2018); published online EpubNov
554   (10.1002/wrna.1491).
555   10.   L. R. Kenner, A. A. Anand, H. C. Nguyen, A. G. Myasnikov, C. J. Klose, L. A. McGeever,
556   J. C. Tsai, L. E. Miller-Vedam, P. Walter, A. Frost, eIF2B-catalyzed nucleotide exchange
557   and phosphoregulation by the integrated stress response. *Science* **364**, 491-495 (2019);
558   published online EpubMay 3 (10.1126/science.aaw2922).
559   11.   K. Pakos-Zebrucka, I. Koryga, K. Mnich, M. Ljujic, A. Samali, A. M. Gorman, The
560   integrated stress response. *EMBO Rep* **17**, 1374-1395 (2016); published online EpubOct
561   (10.15252/embr.201642195).
562   12.   O. J. Freeman, G. R. Mallucci, The UPR and synaptic dysfunction in neurodegeneration.
563   *Brain   Res*   **1648**,   530-537   (2016);   published   online   EpubOct   1
564   (10.1016/j.brainres.2016.03.029).
565   13.   J. F. Abisambra, U. K. Jinwal, L. J. Blair, J. C. O'Leary, 3rd, Q. Li, S. Brady, L. Wang, C.
566   E. Guidi, B. Zhang, B. A. Nordhues, M. Cockman, A. Suntharalingham, P. Li, Y. Jin, C.
567   A. Atkins, C. A. Dickey, Tau accumulation activates the unfolded protein response by
568   impairing endoplasmic reticulum-associated degradation. *J Neurosci* **33**, 9498-9507
569   (2013); published online EpubMay 29 (10.1523/JNEUROSCI.5397-12.2013).
570   14.   J. A. Moreno, H. Radford, D. Peretti, J. R. Steinert, N. Verity, M. G. Martin, M. Halliday,
571   J. Morgan, D. Dinsdale, C. A. Ortori, D. A. Barrett, P. Tsaytler, A. Bertolotti, A. E. Willis,
572   M. Bushell, G. R. Mallucci, Sustained translational repression by eIF2alpha-P mediates
573   prion neurodegeneration. *Nature* **485**, 507-511 (2012); published online EpubMay 24
574   (10.1038/nature11058).
575   15.   M. V. Lourenco, J. R. Clarke, R. L. Frozza, T. R. Bomfim, L. Forny-Germano, A. F.
576   Batista, L. B. Sathler, J. Brito-Moreira, O. B. Amaral, C. A. Silva, L. Freitas-Correa, S.
577   Espirito-Santo, P. Campello-Costa, J. C. Houzel, W. L. Klein, C. Holscher, J. B.
578   Carvalheira, A. M. Silva, L. A. Velloso, D. P. Munoz, S. T. Ferreira, F. G. De Felice, TNF-
579   alpha mediates PKR-dependent memory impairment and brain IRS-1 inhibition induced
580   by Alzheimer's beta-amyloid oligomers in mice and monkeys. *Cell Metab* **18**, 831-843
581   (2013); published online EpubDec 3 (10.1016/j.cmet.2013.11.002).
582   16.   T. Ma, M. A. Trinh, A. J. Wexler, C. Bourbon, E. Gatti, P. Pierre, D. R. Cavener, E. Klann,
583   Suppression of eIF2alpha kinases alleviates Alzheimer's disease-related plasticity and
584   memory deficits. *Nat Neurosci* **16**, 1299-1305 (2013); published online EpubSep
585   (10.1038/nn.3486).
586   17.   J. Baleriola, C. A. Walker, Y. Y. Jean, J. F. Crary, C. M. Troy, P. L. Nagy, U. Hengst,
587   Axonally synthesized ATF4 transmits a neurodegenerative signal across brain regions. *Cell*
588   **158**, 1159-1172 (2014); published online EpubAug 28 (10.1016/j.cell.2014.07.001).
589   18.   M. Halliday, H. Radford, Y. Sekine, J. Moreno, N. Verity, J. le Quesne, C. A. Ortori, D.
590   A. Barrett, C. Fromont, P. M. Fischer, H. P. Harding, D. Ron, G. R. Mallucci, Partial
591   restoration of protein synthesis rates by the small molecule ISRIB prevents
592   neurodegeneration   without   pancreatic   toxicity.   *Cell   Death   Dis*   **6**,   e1672
593   (2015)10.1038/cddis.2015.49).
594   19.   A. Chou, K. Krukowski, T. Jopson, P. J. Zhu, M. Costa-Mattioli, P. Walter, S. Rosi,
595   Inhibition of the integrated stress response reverses cognitive deficits after traumatic brain
596   injury. *Proc Natl Acad Sci U S A* **114**, E6420-E6426 (2017); published online EpubAug 1
597   (10.1073/pnas.1707661114).

20. W. Cheng, S. Wang, A. A. Mestre, C. Fu, A. Makarem, F. Xian, L. R. Hayes, R. Lopez-Gonzalez, K. Drenner, J. Jiang, D. W. Cleveland, S. Sun, C9ORF72 GGGGCC repeat-associated non-AUG translation is upregulated by stress through eIF2alpha phosphorylation. *Nat Commun* **9**, 51 (2018); published online EpubJan 4 (10.1038/s41467-017-02495-z).

21. G. Martinez, S. Khatiwada, M. Costa-Mattioli, C. Hetz, ER Proteostasis Control of Neuronal Physiology and Synaptic Function. *Trends Neurosci* **41**, 610-624 (2018); published online EpubSep (10.1016/j.tins.2018.05.009).

22. Y. L. Wong, L. LeBon, A. M. Basso, K. L. Kohlhaas, A. L. Nikkel, H. M. Robb, D. L. Donnelly-Roberts, J. Prakash, A. M. Swensen, N. D. Rubinstein, S. Krishnan, F. E. McAllister, N. V. Haste, J. J. O'Brien, M. Roy, A. Ireland, J. M. Frost, L. Shi, S. Riedmaier, K. Martin, M. J. Dart, C. Sidrauski, eIF2B activator prevents neurological defects caused by a chronic integrated stress response. *Elife* **8**, (2019); published online EpubJan 9 (10.7554/eLife.42940).

23. P. J. Zhu, S. Khatiwada, Y. Cui, L. C. Reineke, S. W. Dooling, J. J. Kim, W. Li, P. Walter, M. Costa-Mattioli, Activation of the ISR mediates the behavioral and neurophysiological abnormalities in Down syndrome. *Science* **366**, 843-849 (2019); published online EpubNov 15 (10.1126/science.aaw5185).

24. R. C. Chang, A. K. Wong, H. K. Ng, J. Hugon, Phosphorylation of eukaryotic initiation factor-2alpha (eIF2alpha) is associated with neuronal degeneration in Alzheimer's disease. *Neuroreport* **13**, 2429-2432 (2002); published online EpubDec 20 (10.1097/00001756-200212200-00011).

25. G. Page, A. Rioux Bilan, S. Ingrand, C. Lafay-Chebassier, S. Pain, M. C. Perault Pochat, C. Bouras, T. Bayer, J. Hugon, Activated double-stranded RNA-dependent protein kinase and neuronal death in models of Alzheimer's disease. *Neuroscience* **139**, 1343-1354 (2006)10.1016/j.neuroscience.2006.01.047).

26. Y. Segev, I. Barrera, H. Ounallah-Saad, K. Wibrand, I. Sporild, A. Livne, T. Rosenberg, O. David, M. Mints, C. R. Bramham, K. Rosenblum, PKR Inhibition Rescues Memory Deficit and ATF4 Overexpression in ApoE epsilon4 Human Replacement Mice. *J Neurosci* **35**, 12986-12993 (2015); published online EpubSep 23 (10.1523/JNEUROSCI.5241-14.2015).

27. C. Sidrauski, D. Acosta-Alvear, A. Khoutorsky, P. Vedantham, B. R. Hearn, H. Li, K. Gamache, C. M. Gallagher, K. K. Ang, C. Wilson, V. Okreglak, A. Ashkenazi, B. Hann, K. Nader, M. R. Arkin, A. R. Renslo, N. Sonenberg, P. Walter, Pharmacological brake-release of mRNA translation enhances cognitive memory. *Elife* **2**, e00498 (2013)10.7554/eLife.00498).

28. C. Sidrauski, J. C. Tsai, M. Kampmann, B. R. Hearn, P. Vedantham, P. Jaishankar, M. Sokabe, A. S. Mendez, B. W. Newton, E. L. Tang, E. Verschueren, J. R. Johnson, N. J. Krogan, C. S. Fraser, J. S. Weissman, A. R. Renslo, P. Walter, Pharmacological dimerization and activation of the exchange factor eIF2B antagonizes the integrated stress response. *Elife* **4**, e07314 (2015)10.7554/eLife.07314).

29. Y. Sekine, A. Zyryanova, A. Crespillo-Casado, P. M. Fischer, H. P. Harding, D. Ron, Stress responses. Mutations in a translation initiation factor identify the target of a memory-enhancing compound. *Science* **348**, 1027-1030 (2015); published online EpubMay 29 (10.1126/science.aaa6986).

26

30. S. T. Ferreira, M. V. Lourenco, M. M. Oliveira, F. G. De Felice, Soluble amyloid-beta oligomers as synaptotoxins leading to cognitive impairment in Alzheimer's disease. *Front Cell Neurosci* **9**, 191 (2015)10.3389/fncel.2015.00191).

31. C. P. Figueiredo, J. R. Clarke, J. H. Ledo, F. C. Ribeiro, C. V. Costa, H. M. Melo, A. P. Mota-Sales, L. M. Saraiva, W. L. Klein, A. Sebollela, F. G. De Felice, S. T. Ferreira, Memantine rescues transient cognitive impairment caused by high-molecular-weight abeta oligomers but not the persistent impairment induced by low-molecular-weight oligomers. *J Neurosci* **33**, 9626-9634 (2013); published online EpubJun 5 (10.1523/JNEUROSCI.0482-13.2013).

32. M. V. Lourenco, R. L. Frozza, G. B. de Freitas, H. Zhang, G. C. Kincheski, F. C. Ribeiro, R. A. Goncalves, J. R. Clarke, D. Beckman, A. Staniszewski, H. Berman, L. A. Guerra, L. Forny-Germano, S. Meier, D. M. Wilcock, J. M. de Souza, S. Alves-Leon, V. F. Prado, M. A. M. Prado, J. F. Abisambra, F. Tovar-Moll, P. Mattos, O. Arancio, S. T. Ferreira, F. G. De Felice, Exercise-linked FNDC5/irisin rescues synaptic plasticity and memory defects in Alzheimer's models. *Nat Med* **25**, 165-175 (2019); published online EpubJan (10.1038/s41591-018-0275-4).

33. E. K. Schmidt, G. Clavarino, M. Ceppi, P. Pierre, SUnSET, a nonradioactive method to monitor protein synthesis. *Nat Methods* **6**, 275-277 (2009); published online EpubApr (10.1038/nmeth.1314).

34. H. Bowling, A. Bhattacharya, G. Zhang, J. Z. Lebowitz, D. Alam, P. T. Smith, K. Kirshenbaum, T. A. Neubert, C. Vogel, M. V. Chao, E. Klann, BONLAC: A combinatorial proteomic technique to measure stimulus-induced translational profiles in brain slices. *Neuropharmacology* **100**, 76-89 (2016); published online EpubJan (10.1016/j.neuropharm.2015.07.017).

35. J. L. Jankowsky, D. J. Fadale, J. Anderson, G. M. Xu, V. Gonzales, N. A. Jenkins, N. G. Copeland, M. K. Lee, L. H. Younkin, S. L. Wagner, S. G. Younkin, D. R. Borchelt, Mutant presenilins specifically elevate the levels of the 42 residue beta-amyloid peptide in vivo: evidence for augmentation of a 42-specific gamma secretase. *Hum Mol Genet* **13**, 159-170 (2004); published online EpubJan 15 (10.1093/hmg/ddh019).

36. J. J. Hoozemans, R. Veerhuis, E. S. Van Haastert, J. M. Rozemuller, F. Baas, P. Eikelenboom, W. Scheper, The unfolded protein response is activated in Alzheimer's disease. *Acta Neuropathol* **110**, 165-172 (2005); published online EpubAug (10.1007/s00401-005-1038-0).

37. M. Tible, F. Mouton Liger, J. Schmitt, A. Giralt, K. Farid, S. Thomasseau, S. Gourmaud, C. Paquet, L. Rondi Reig, E. Meurs, J. A. Girault, J. Hugon, PKR knockout in the 5xFAD model of Alzheimer's disease reveals beneficial effects on spatial memory and brain lesions. *Aging Cell* **18**, e12887 (2019); published online EpubJun (10.1111/acel.12887).

38. R. Bugallo, E. Marlin, A. Baltanas, E. Toledo, R. Ferrero, R. Vinueza-Gavilanes, L. Larrea, M. Arrasate, T. Aragon, Fine tuning of the unfolded protein response by ISRIB improves neuronal survival in a model of amyotrophic lateral sclerosis. *Cell Death Dis* **11**, 397 (2020); published online EpubMay 26 (10.1038/s41419-020-2601-2).

39. Z. D. Kabir, A. Che, D. K. Fischer, R. C. Rice, B. K. Rizzo, M. Byrne, M. J. Glass, N. V. De Marco Garcia, A. M. Rajadhyaksha, Rescue of impaired sociability and anxiety-like behavior in adult cacna1c-deficient mice by pharmacologically targeting eIF2alpha. *Mol Psychiatry* **22**, 1096-1109 (2017); published online EpubAug (10.1038/mp.2017.124).

688 40. D. I. Briggs, E. Defensor, P. Memar Ardestani, B. Yi, M. Halpain, G. Seabrook, M.
689 Shamloo, Role of Endoplasmic Reticulum Stress in Learning and Memory Impairment and
690 Alzheimer's Disease-Like Neuropathology in the PS19 and APP(Swe) Mouse Models of
691 Tauopathy and Amyloidosis. *eNeuro* **4**, (2017); published online EpubJul-Aug
692 (10.1523/ENEURO.0025-17.2017).

693 41. P. Shrestha, P. Ayata, P. Herrero-Vidal, F. Longo, A. Gastone, J. E. LeDoux, N. Heintz, E.
694 Klann, Cell-type-specific drug-inducible protein synthesis inhibition demonstrates that
695 memory consolidation requires rapid neuronal translation. *Nat Neurosci* **23**, 281-292
696 (2020); published online EpubFeb (10.1038/s41593-019-0568-z).

697 42. H. H. Rabouw, M. A. Langereis, A. A. Anand, L. J. Visser, R. J. de Groot, P. Walter, F. J.
698 M. van Kuppeveld, Small molecule ISRIB suppresses the integrated stress response within
699 a defined window of activation. *Proc Natl Acad Sci U S A* **116**, 2097-2102 (2019);
700 published online EpubFeb 5 (10.1073/pnas.1815767116).

701 43. M. Costa-Mattioli, P. Walter, The integrated stress response: From mechanism to disease.
702 *Science* **368**, (2020); published online EpubApr 24 (10.1126/science.aat5314).

703 44. S. Dey, T. D. Baird, D. Zhou, L. R. Palam, D. F. Spandau, R. C. Wek, Both transcriptional
704 regulation and translational control of ATF4 are central to the integrated stress response. *J
705 Biol Chem* **285**, 33165-33174 (2010); published online EpubOct 22
706 (10.1074/jbc.M110.167213).

707 45. B. F. Teske, S. A. Wek, P. Bunpo, J. K. Cundiff, J. N. McClintick, T. G. Anthony, R. C.
708 Wek, The eIF2 kinase PERK and the integrated stress response facilitate activation of
709 ATF6 during endoplasmic reticulum stress. *Mol Biol Cell* **22**, 4390-4405 (2011); published
710 online EpubNov (10.1091/mbc.E11-06-0510).

711 46. H. Mathys, J. Davila-Velderrain, Z. Peng, F. Gao, S. Mohammadi, J. Z. Young, M. Menon,
712 L. He, F. Abdurrob, X. Jiang, A. J. Martorell, R. M. Ransohoff, B. P. Hafler, D. A. Bennett,
713 M. Kellis, L. H. Tsai, Single-cell transcriptomic analysis of Alzheimer's disease. *Nature*
714 **570**, 332-337 (2019); published online EpubJun (10.1038/s41586-019-1195-2).

715 47. J. C. Tsai, L. E. Miller-Vedam, A. A. Anand, P. Jaishankar, H. C. Nguyen, A. R. Renslo,
716 A. Frost, P. Walter, Structure of the nucleotide exchange factor eIF2B reveals mechanism
717 of memory-enhancing molecule. *Science* **359**, (2018); published online EpubMar 30
718 (10.1126/science.aaq0939).

719 48. M. Halliday, H. Radford, K. A. M. Zents, C. Molloy, J. A. Moreno, N. C. Verity, E. Smith,
720 C. A. Ortori, D. A. Barrett, M. Bushell, G. R. Mallucci, Repurposed drugs targeting eIF2α-
721 P-mediated translational repression prevent neurodegeneration in mice. *Brain* **140**, 1768-
722 1783 (2017); published online EpubJun 1 (10.1093/brain/awx074).

723 49. M. P. Lambert, A. K. Barlow, B. A. Chromy, C. Edwards, R. Freed, M. Liosatos, T. E.
724 Morgan, I. Rozovsky, B. Trommer, K. L. Viola, P. Wals, C. Zhang, C. E. Finch, G. A.
725 Krafft, W. L. Klein, Diffusible, nonfibrillar ligands derived from Abeta1-42 are potent
726 central nervous system neurotoxins. *Proc Natl Acad Sci U S A* **95**, 6448-6453 (1998);
727 published online EpubMay 26 (10.1073/pnas.95.11.6448).

728 50. A. Sebollela, L. Freitas-Correa, F. F. Oliveira, A. C. Paula-Lima, L. M. Saraiva, S. M.
729 Martins, L. D. Mota, C. Torres, S. Alves-Leon, J. M. de Souza, D. M. Carraro, H. Brentani,
730 F. G. De Felice, S. T. Ferreira, Amyloid-beta oligomers induce differential gene expression
731 in adult human brain slices. *J Biol Chem* **287**, 7436-7445 (2012); published online
732 EpubMar 2 (10.1074/jbc.M111.298471).

28

733 51. T. D. Schmittgen, K. J. Livak, Analyzing real-time PCR data by the comparative C(T)
734   method. *Nat Protoc* **3**, 1101-1108 (2008)10.1038/nprot.2008.73).
735 52. D. C. Dieterich, A. J. Link, J. Graumann, D. A. Tirrell, E. M. Schuman, Selective
736   identification of newly synthesized proteins in mammalian cells using bioorthogonal
737   noncanonical amino acid tagging (BONCAT). *Proc Natl Acad Sci U S A* **103**, 9482-9487
738   (2006); published online EpubJun 20 (10.1073/pnas.0601637103).
739 53. J. H. Ledo, E. P. Azevedo, J. R. Clarke, F. C. Ribeiro, C. P. Figueiredo, D. Foguel, F. G.
740   De Felice, S. T. Ferreira, Amyloid-beta oligomers link depressive-like behavior and
741   cognitive deficits in mice. *Mol Psychiatry* **18**, 1053-1054 (2013); published online
742   EpubOct (10.1038/mp.2012.168).
743 54. F. Trinchese, M. Fa, S. Liu, H. Zhang, A. Hidalgo, S. D. Schmidt, H. Yamaguchi, N.
744   Yoshii, P. M. Mathews, R. A. Nixon, O. Arancio, Inhibition of calpains improves memory
745   and synaptic transmission in a mouse model of Alzheimer disease. *J Clin Invest* **118**, 2796-
746   2807 (2008); published online EpubAug (10.1172/JCI34254).
747 55. J. L. Banko, F. Poulin, L. Hou, C. T. DeMaria, N. Sonenberg, E. Klann, The translation
748   repressor 4E-BP2 is critical for eIF4F complex formation, synaptic plasticity, and memory
749   in the hippocampus. *J Neurosci* **25**, 9581-9590 (2005); published online EpubOct 19
750   (10.1523/JNEUROSCI.2423-05.2005).
751 56. W. Yang, X. Zhou, H. R. Zimmermann, D. R. Cavener, E. Klann, T. Ma, Repression of the
752   eIF2alpha kinase PERK alleviates mGluR-LTD impairments in a mouse model of
753   Alzheimer's disease. *Neurobiol Aging* **41**, 19-24 (2016); published online EpubMay
754   (10.1016/j.neurobiolaging.2016.02.005).

778

779   **Figure legends**

780

781   **Figure 1. AD brains display increased eIF2α-P and reduced levels of eIF2B**

782   **subunits.** Cortical tissue from AD subjects and age-matched controls were probed for

783   translation initiation factors. Samples were probed for eIF2α-P (A; F = 3.125; N = 7 Control

784   cases; N = 7 AD cases), total eIF2α (B; F = 1.319; N = 8 Control cases; N = 8 AD cases),

785   eIF2γ (C; F = 1.547; N = 8 Control cases; N = 7 AD cases), eIF2Bα (D; F = 1.375; N = 8

786   Control cases; N = 8 AD cases) and eIF2Bϵ (E; F = 2.823; N = 8 Control cases; N = 7 AD

787   cases) by Western blotting (AD). eIF2α-P was normalized by total eIF2α. eIF2α, eIF2γ,

788   eIF2Bα and eIF2Bϵ were normalized by GAPDH. Non-contiguous lanes from the same

789   blot are shown in C, D and E. Outliers were excluded from each analysis using Grubb's

790   test (α = 0.05) from GraphPad Prism 6. *p < 0.05; **p < 0.01; Two-tailed unpaired *t*-test.

791   Dots represent individual subjects.

792

793   **Figure 2. Systemic treatment with ISRIB prevents memory impairment induced by**

794   **eIF2α-P.** (A) ISRIB concentrations in plasma and brain were determined by mass

795   spectrometry 4 or 24 hours after i.p. administration (0.25 mg/kg for 6 consecutive days)

796   in mice (N = 4 mice/time point). (B) Experimental timeline: C57BL/6 mice were treated

797   with salubrinal alone (10 mg/kg, i.p.; orange arrows) or salubrinal + ISRIB (0.25 mg/kg,

798   i.p.; black arrows) on days 1-5, 7, 9-11. Mice were trained and tested in the Novel Object

799   Recognition (NOR) task on days 6 and 7, respectively, and were trained and tested in the

800   Contextual Fear Conditioning (CFC) task on days 8 and 9, respectively. Brains were

801   collected on day 12. (C) Discrimination index in the NOR test (F = 12.00; N = 5-7

802   mice/group;). (D) Freezing time in the CFC test (F = 5.049; N = 5-7 mice/group). (E)

803   Hippocampal eIF2α-P in mice treated with salubrinal alone or salubrinal + ISRIB,

804   normalized by total eIF2α (N = 6-7 mice/group; F = 5.461). In all panels, dots correspond

805   to individual mice. *p < 0.05, **p < 0.01, ***p<0.001, One-way ANOVA followed by

806   Dunnet's *post hoc* test.

807

808   **Figure 3. ISRIB prevents memory impairments, dendritic spine loss and defective**

809   **hippocampal protein synthesis induced by AβOs.** (A) Experimental timeline: C57BL/6

810   mice received an i.c.v. infusion of AβOs (10 pmol; orange arrow) and were treated with

811   ISRIB (0.25 mg/kg, i.p.; black arrows) or saline on days 1-5, 7, 9-11. Mice were trained

812   and tested in the Novel Object Recognition (NOR) task on days 6 and 7, respectively,

31

813   and were trained and tested in the Contextual Fear Conditioning (CFC) task on days 8

814   and 9, respectively. Brains were collected on day 12. (B) eIF2α-P in the hippocampi of

815   mice that received an i.c.v infusion of AβOs (or vehicle) and were treated with ISRIB (0.25

816   mg/kg, i.p., for 5 days) or saline (N = 8-9 mice/group). (C) ATF4 in the hippocampi of mice

817   that received an i.c.v infusion of AβOs (or vehicle) and were treated with ISRIB (0.25

818   mg/kg, i.p., for 5 days) or saline (N = 10-12 mice/group). (D) Mouse hippocampal slices

819   were exposed to AβOs (1 μM) in the absence or presence of ISRIB (0.2 μM) for 3h and

820   protein synthesis was measured using SUnSET (N = 15-18 slices from a total of 15 mice

821   per experimental condition). Representative images shown had brightness linearly

822   adjusted for clearer visualization. (E) Primary hippocampal cultures were exposed to

823   AβOs (0.5 μM) in the absence or presence of ISRIB (0.2 μM) for 3h, and newly

824   synthesized proteins were detected by BONCAT (labeling with AHA followed by Click

825   chemistry for biotinylation of AHA-containing polypeptides; see "Methods"). After

826   pulldown with streptavidin-conjugated resin, proteins were detected by Western blotting.

827   Symbols represent experiments with independent hippocampal cultures and independent

828   AβO preparations (N = 3 independent primary cultures). (F) Dendritic spine density was

829   analyzed in apical dendrites of neurons from the CA1 region of the hippocampus. Each

830   symbol corresponds to the mean of three independent 20 μm segments per neuron, 5

831   neurons per mouse (N = 4-5 mice/group). (G) Discrimination index in the NOR test (F =

832   5.468; N = 14-17 mice/group). (H) Freezing time in the CFC test (F Interaction = 5.683;

833   N = 11-13 mice/group). *$p < 0.05$, **$p < 0.01$, Two-way ANOVA followed by Dunnet's *post*

834   *hoc* test for all experiments, except in panels 3I and 3J, analyzed by One-Way ANOVA

835   followed by Dunnet's *post-hoc* test. Dots represent individual mice.

32

836

837 **Figure 4. ISRIB reverses defective hippocampal LTP and memory in**

838 **APPswe/PS1ΔE9 mice.** 10-13 month-old APPswe/PS1ΔE9 mice (or WT littermates)

839 were treated daily for 2 weeks with ISRIB (0.25 mg/kg, i.p.) prior to behavioral analysis.

840 (A) Field excitatory post-synaptic potential recordings in acute hippocampal slices from

841 WT or APPswe/PS1ΔE9 mice exposed to vehicle or 0.2 µM ISRIB (N = 13-26 slices from

842 6-9 mice/group). (B) On top - Representative slopes for fEPSP measurements. "1" is

843 representative of the baseline, and "2" is representative of potentiation. Graph is

844 representative of field excitatory post-synaptic potentials 90 min after tetanic stimulation.

845 (C) Dendritic spine density was analyzed in apical dendrites of neurons from the CA1

846 region of the hippocampus. Each dot is representative of one segment using in the

847 analysis (N = 4 mice/group) (D) Mice were trained for 5 days in the MWM, and latency

848 time to reach the platform was recorded (N = 10-15 mice/group). Symbols represent

849 means ± SE of the latency times to find the platform on each consecutive day of training.

850 (E) On the 6th day, the platform was removed, and mice were allowed to freely explore

851 the pool for 1 minute. Total time spent in the target quadrant during the probe trial was

852 measured (N = 10-15 mice per group). (F) Contextual fear conditioning of WT or

853 APPswe/PS1ΔE9 mice treated with ISRIB (N = 10-15 mice/group) or saline. (G)

854 Representative photomontage illustrating presence of plaques (6E10 immunoreactivity;

855 green channel) in the dorsal hippocampus of APPSwe/PS1ΔE9 mice treated with vehicle

856 (left) or with ISRIB (right) (N = 4-5 mice/group; scale bar = 200 µm). (H, K) Optical zoom

857 images of regions identified by dashed rectangles in panel G. (I) Average plaque area in

858 the hippocampi of APPswe/PS1ΔE9 mice treated with vehicle or ISRIB (N = 4-5

33

859   mice/group). (J) Total number of plaques normalized by hippocampal area. (L, M) Total

860   Aβ42 measured by ELISA in hippocampal (L) or cortical (M) homogenates of

861   APPSwe/PS1ΔE9 mice treated with vehicle or ISRIB (N = 4 mice/group). *p < 0.05, ****p

862   < 0.0001 Two-way ANOVA followed by Dunnet's *post-hoc* test, except for panel 1A,

863   evaluated by Repeated Measures Two-Way ANOVA, followed by Tukey's *post hoc*
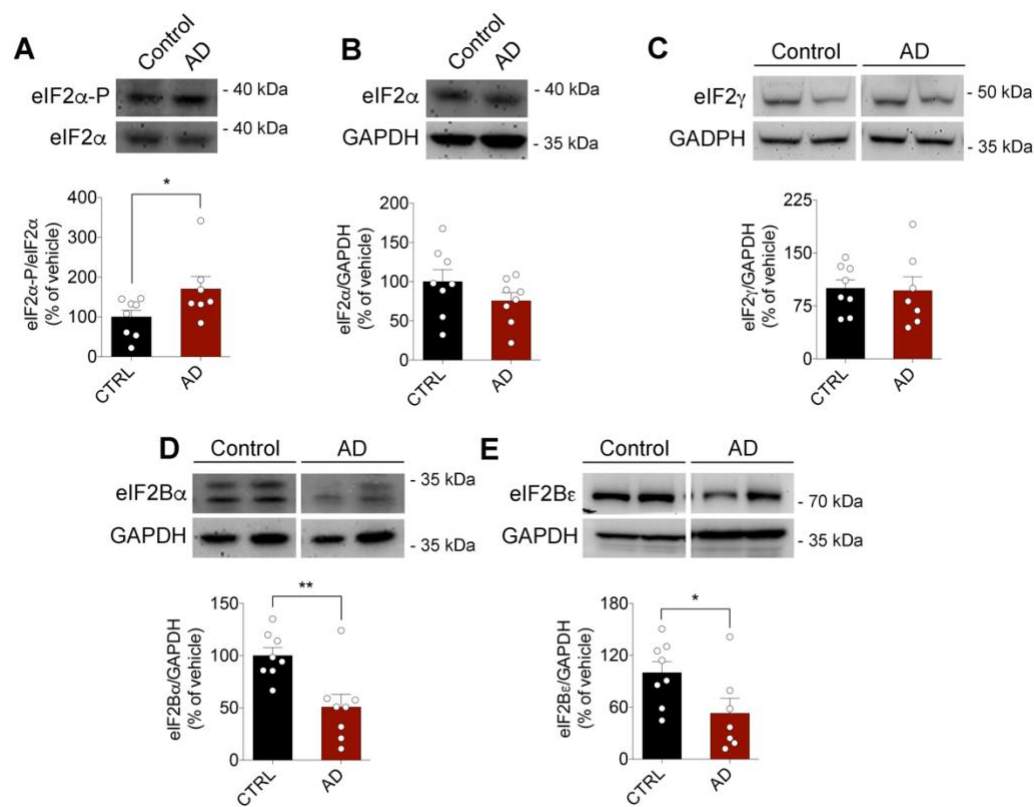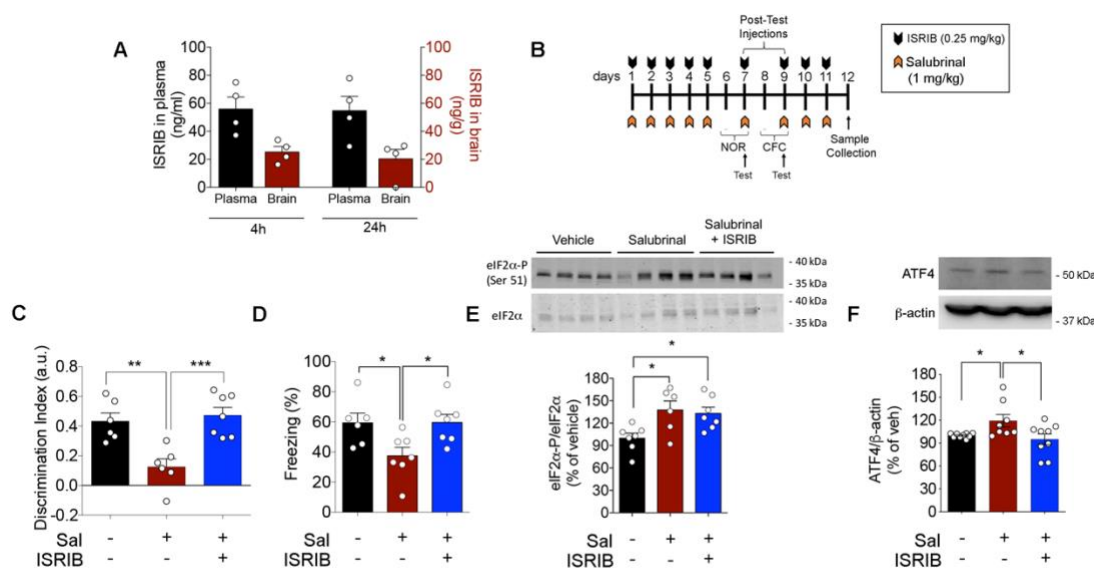
864   analysis. Dots represent individual mice.

Figure 1

Figure 2

Figure 3
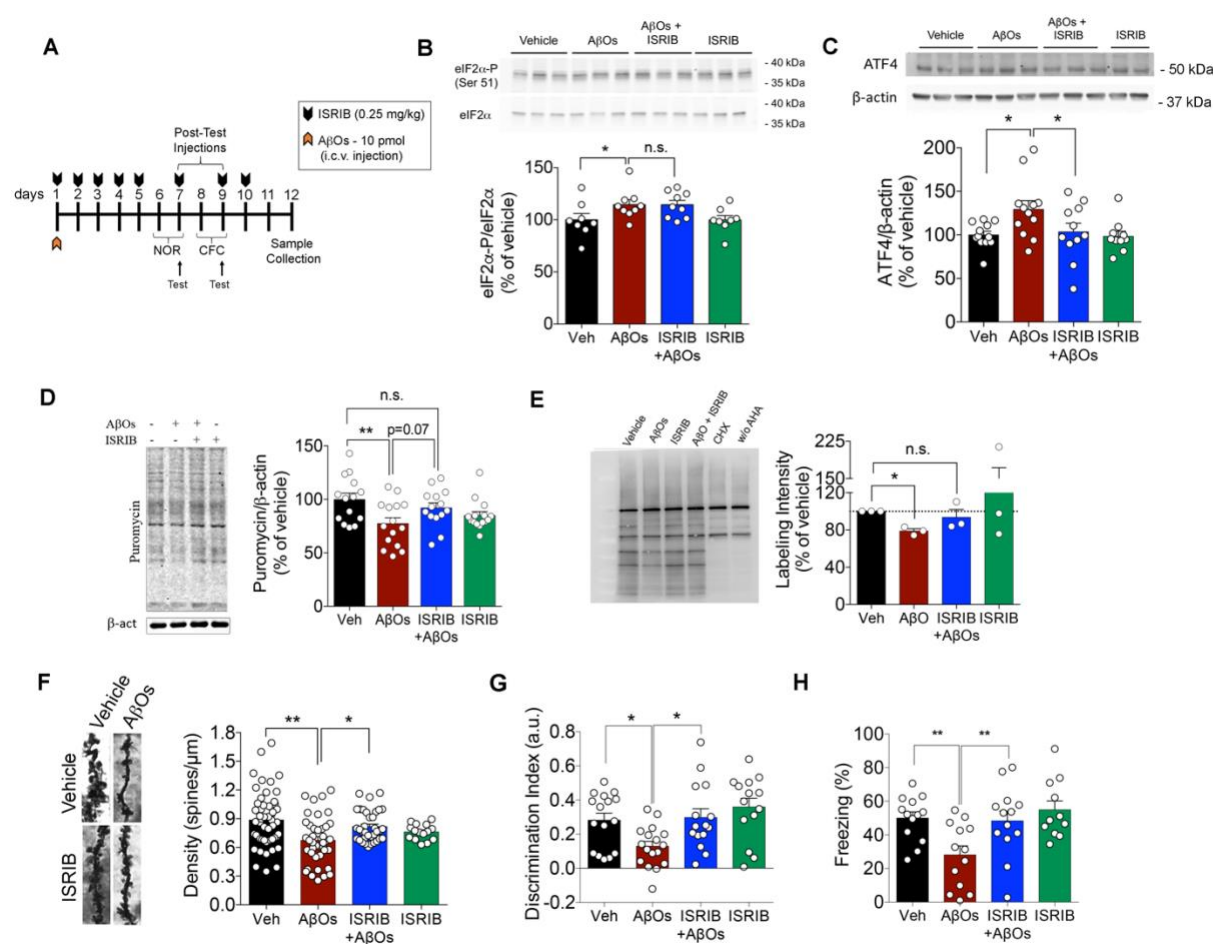
Figure 4
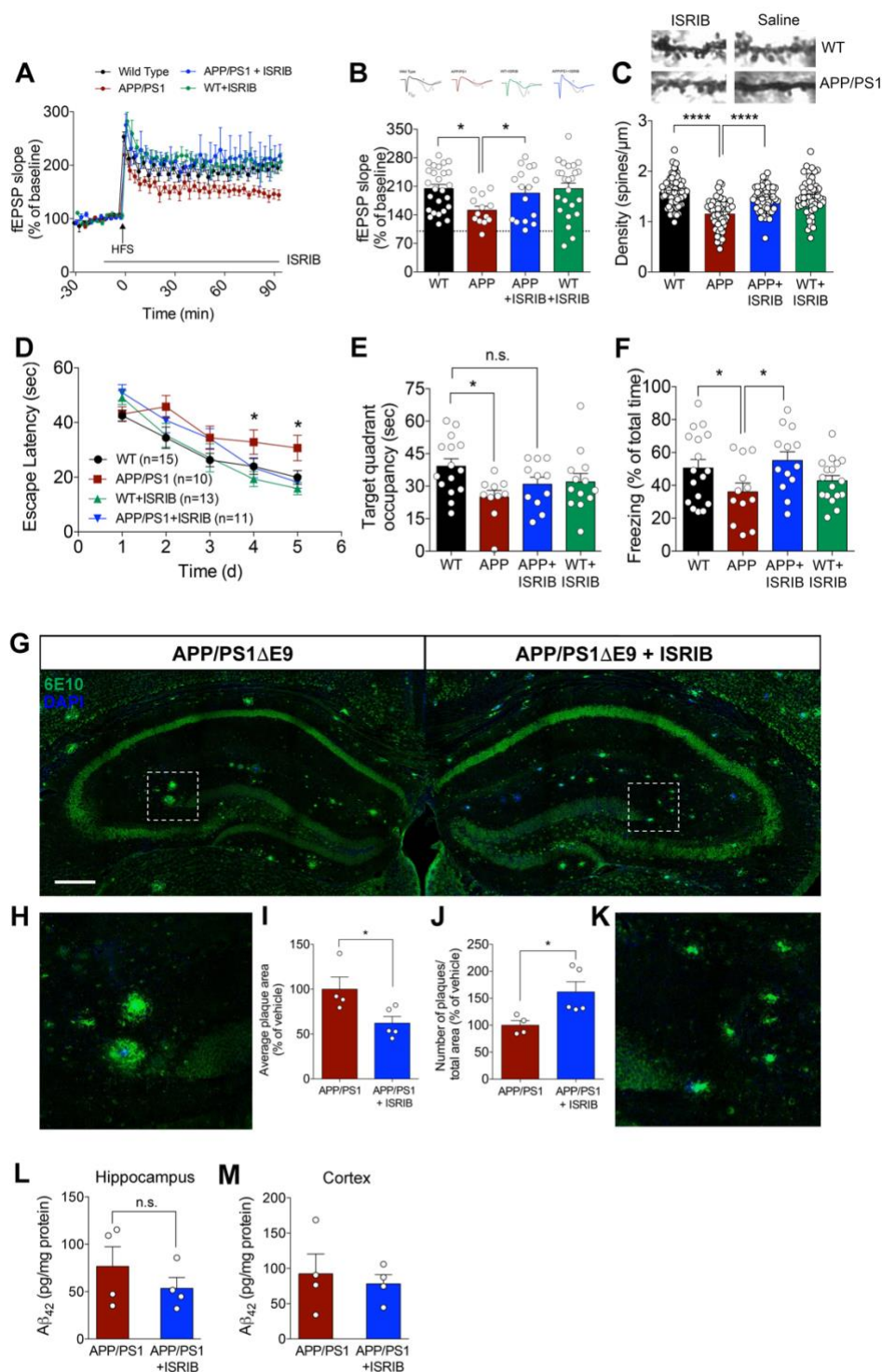
Supplementary Figure 1
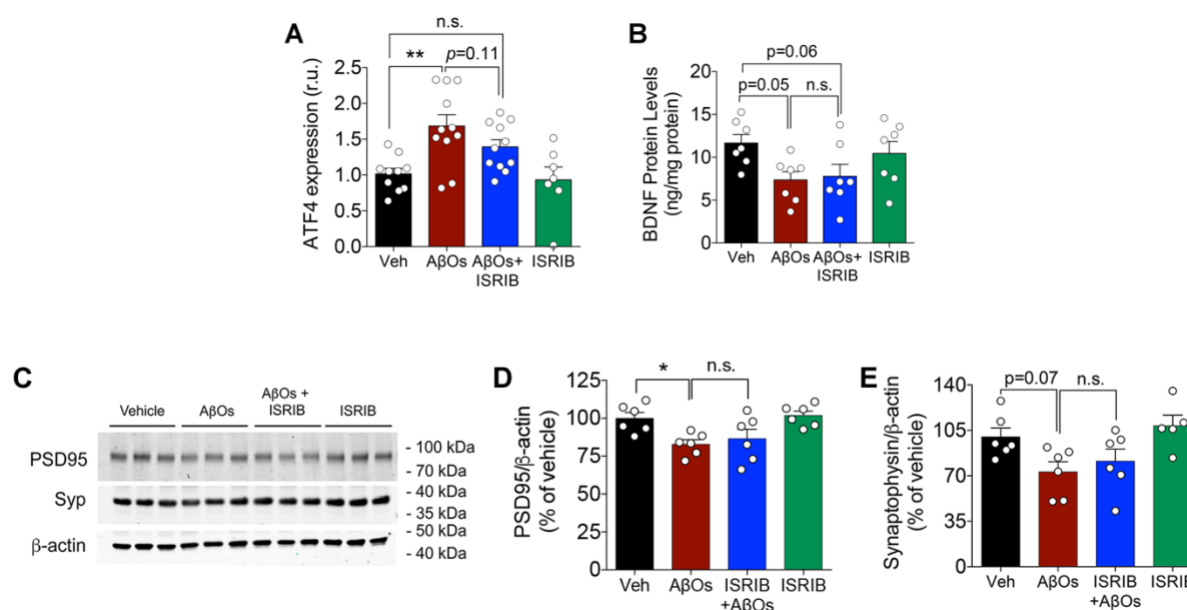
Figure S1. ISRIB does not attenuate the increase in hippocampal ATF4 mRNA, or reductions in BDNF, PSD-95 and synaptophysin protein levels induced by AβOs in mice. Mice received an i.c.v. infusion of 10 pmol AβOs (or vehicle) and were treated daily with ISRIB (0.25 mg/kg, i.p., for 5 days). Hippocampal tissue was collected 12 days after AβO infusion. (A) ATF4 mRNA levels measured by qPCR in the hippocampi of AβO-infused mice treated or not with ISRIB (N = 7-11 mice/group). (B) BDNF measured by ELISA in the hippocampi of the same mice (N = 7 mice/group). (C-E) PSD-95 and synaptophysin levels evaluated by Western blotting in hippocampi of AβO-infused mice and normalized by β-actin levels (N = 6 mice/group). Veh = vehicle. Two-Way ANOVA followed by Dunnet's *post-hoc* test, **$p < 0.01$. Dots represent individual mice.

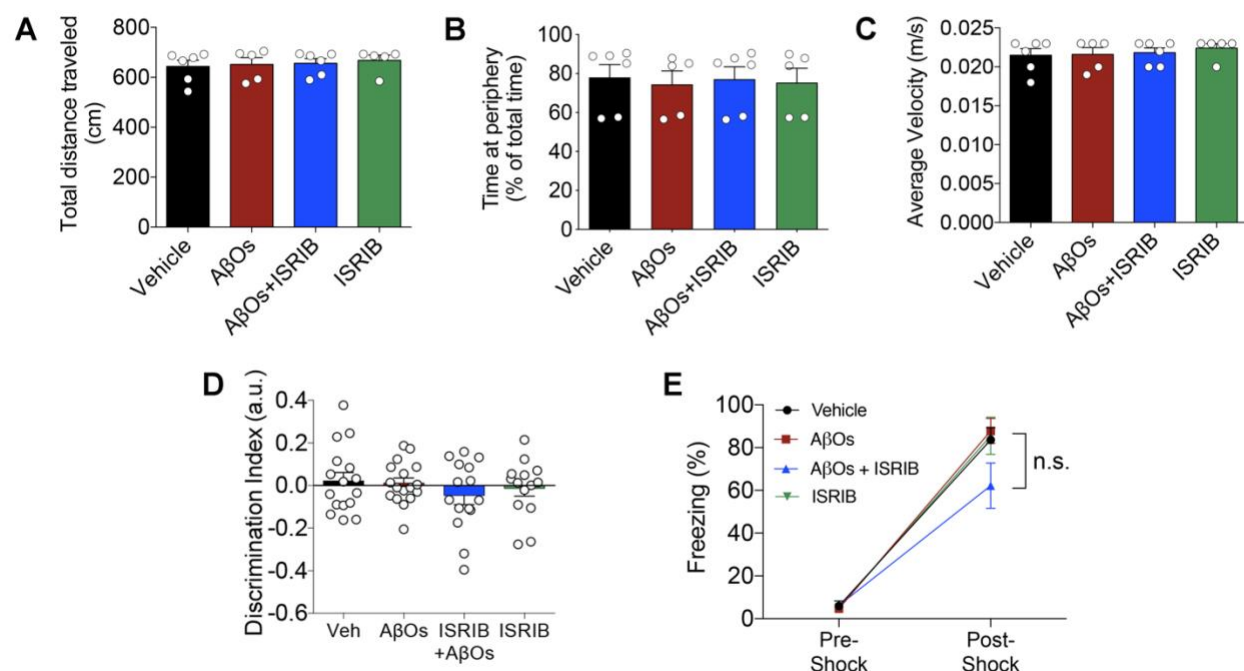**Supplementary Figure 2**

Figure S2. ISRIB does not alter locomotor activities. Mice received an i.c.v. infusion of 10 pmol AβOs and/or were daily treated with ISRIB (0.25 mg/kg; i.p.) as described in Figure 3A. They were allowed to freely explore an open field arena for 5 min, during which total distance traveled (A), time spent at the periphery (B) and average velocity (C) were recorded (N = 5-6 mice/group). (D) Discrimination index of the NOR training session (N = 14-17 mice/group). (E) Freezing behavior during the FC training session, divided in periods pre-shock and post-shock (N = 6-8 mice/group). Veh = vehicle. Two-Way ANOVA followed by Dunnet's *post-hoc* test. Dots correspond to individual mice.
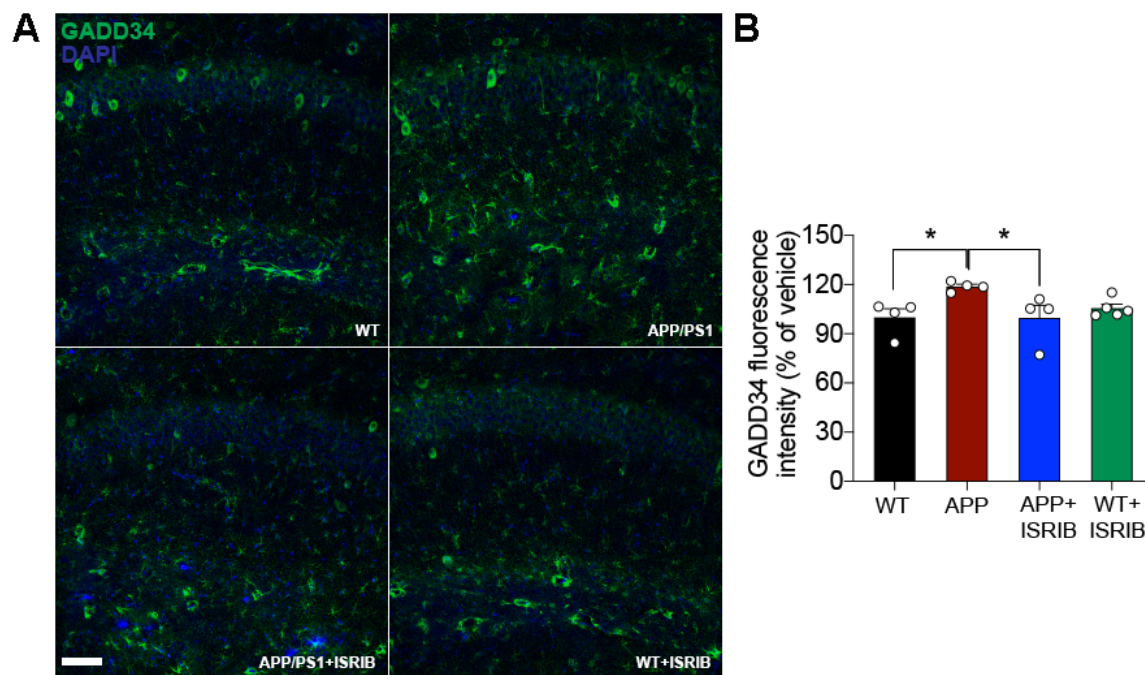
Supplementary Figure 3

Figure S3. ISRIB rescues GADD34 levels in the hippocampus of APPSwe/PS1ΔE9 mice. (A) Representative images of GADD34 levels (green) in the CA1 region from the hippocampus of WT or APPSwe/PS1ΔE9 mice, treated or not with ISRIB (0.25 mg/kg). Scale bar = 20 µm. (B) Quantification of total levels of GADD34 levels in the CA1 region (N = 4-5 mice/group). * = $p <$ 0.05, Two-Way ANOVA followed by Dunnet's test. Dots represent individual mice.
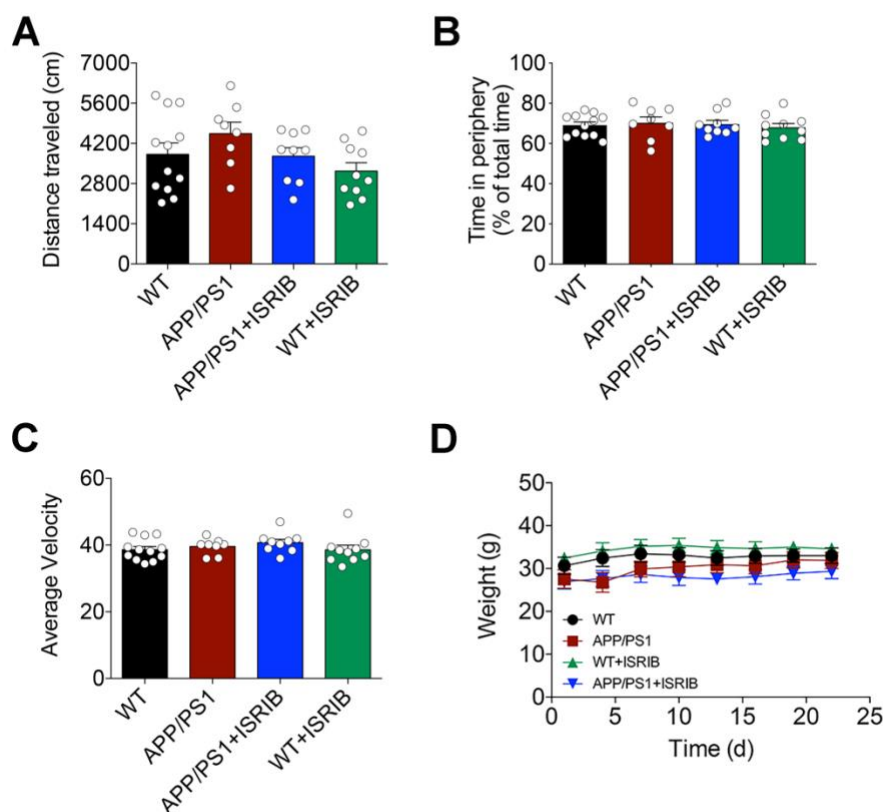
Supplementary Figure 4

Figure S4. Locomotor/exploratory activities and body weight of APPswePS1ΔE9 are not altered by ISRIB treatment. APPswePS1ΔE9 (or WT littermates) mice were treated with ISRIB (0.25 mg/kg, i.p., daily) for 2 weeks prior to behavioral assessment, and during the battery of behavioral tasks (total time of treatment = 24 days). To assess motor and exploratory behaviors, mice were allowed to freely explore an open field arena for 15 min. Total distance traveled (A), percentage of time at the center of the arena (B) and average velocity (C) were measured (N = 8-11 mice/group). (D) Mice were weighted every 3 days for 21 days of treatment (N = 8-11 mice/group). Dots represent individual mice.
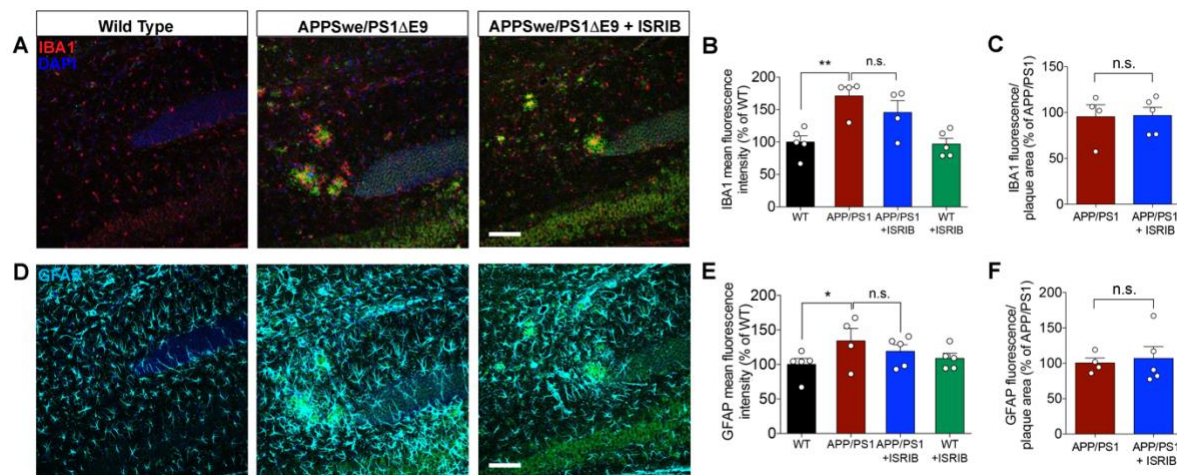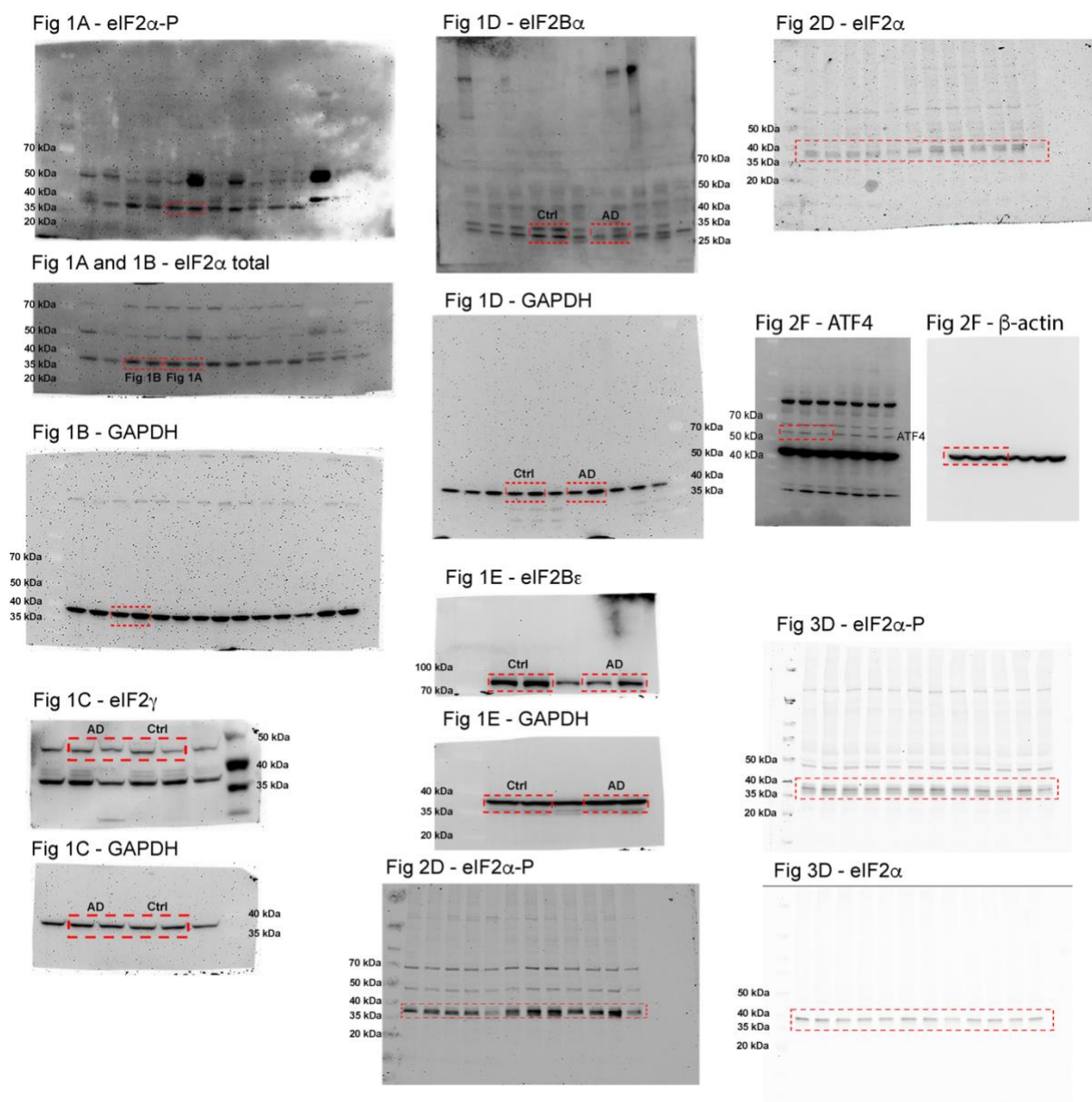
Supplementary Figure 5

Figure S5. Gliosis in APPSwe/PS1ΔE9 hippocampus (dentate gyrus/stratum lacunosum moleculare) is unaffected by ISRIB treatment. (A) Representative Iba-1 immunoreactivity images (red) in the hippocampi of WT, APPSwe/PS1ΔE9 or ISRIB-treated APPSwe/PS1ΔE9 mice (scale bar = 50 µm). (B) Quantitative analysis of Iba-1 immunoreactivity (mean fluorescence intensity; N = 4-5 mice/group). (C) Quantitative analysis of Iba-1 immunoreactivity (mean fluorescence intensity) co-localized with or immediately surrounding plaques (N = 4-5 mice/group). (D) Representative GFAP immunoreactivity images (cyan) in the hippocampi of W, APPSwe/PS1ΔE9 or ISRIB-treated APPSwe/PS1ΔE9 mice (scale bar = 50 µm). (E) Quantitative analysis of GFAP immunoreactivity (mean fluorescence intensity; N = 4-5 mice/group). (F) Quantitative analysis of GFAP immunoreactivity (mean fluorescence intensity) co-localized with or immediately surrounding plaques (N = 4-5 mice/group). n.s. = not statistically significant. *p<0.05, **p<0.01, Two-Way ANOVA followed by Fisher's test. Dots represent individual mice.
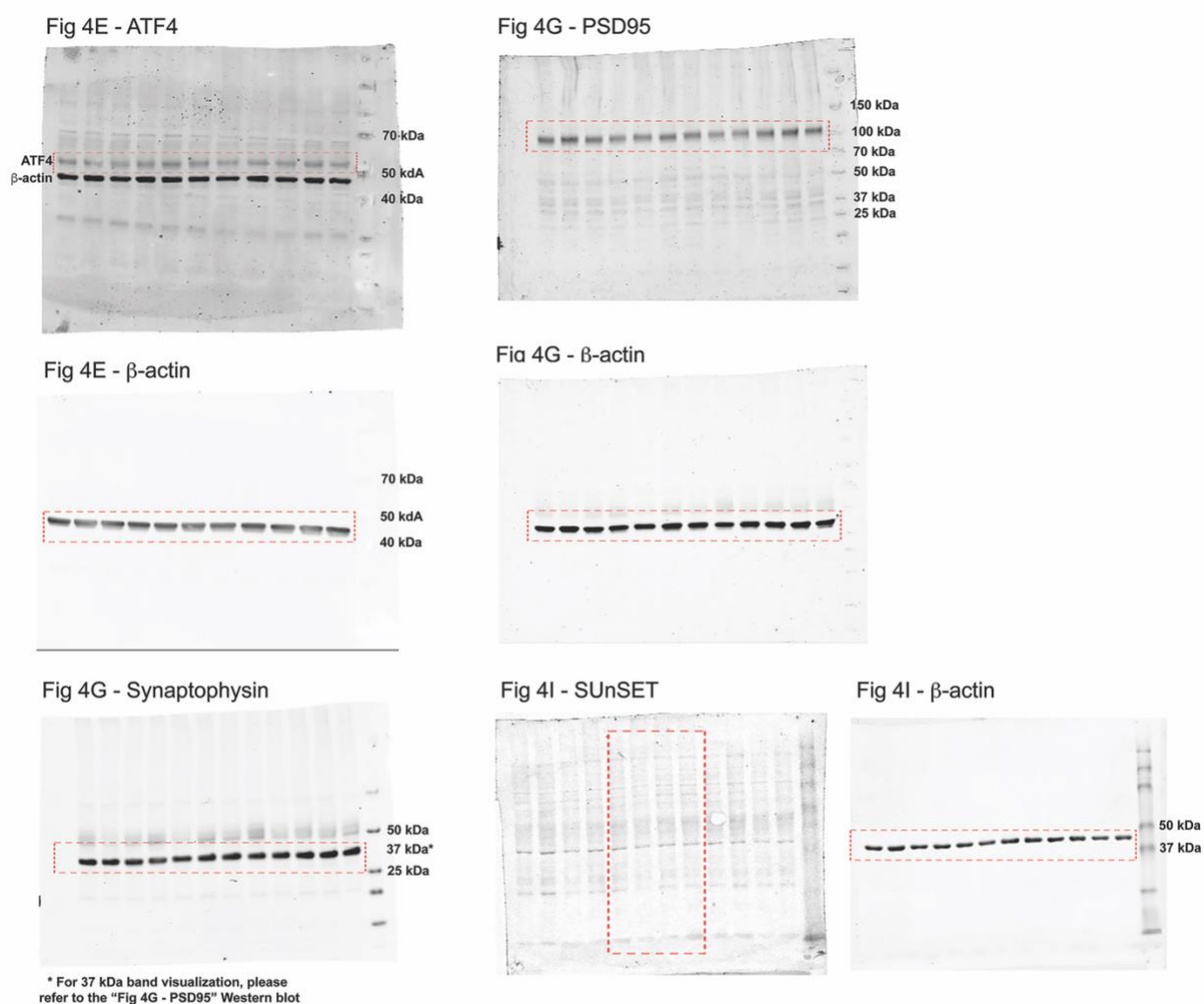
Supplementary Figure 6

Fig S6. Full Western blots used in the current study. Lanes shown in main figures are boxed in red.

Supplementary Table 1. Demographics of control and AD brains.

Case Number	Primary Neuropathologic Diagnosis	PMI (hr)	Age at Onset	Age at Death	ApoE	Sex
OS02-252	AD	17		50	E3/3	Female
OS00-11	AD	4	49	55	E3/3	Male
E06-154	AD	5	52	60	E4/4	Male
OS-140909	AD	6	51	61	E3/3	Female
OS02-163	AD	11	53	70	E3/4	Male
E08-53	AD	8	70	78	E3/3	Female
E10-149	AD	6.5	77	90	E2/4	Male
E08-108	AD	4	76	94	E3/4	Female
E05-130	Control	3	N/A	52	E3/4	Female
E14-06	Control	12.5	N/A	56		Male
E05-74	Control	6	N/A	59	E2/3	Male
E15-106	Control	6	N/A	61		Female
E16-45	Control	2.5	N/A	70	E3/3	Male
E08-101	Control	11.5	N/A	78	E3/3	Female
E13-27	Control	6	N/A	91	E3/3	Female
E10-142	Control	5.5	N/A	94	E3/3	Male

PMI: post-mortem interval

ApoE: Apolipoprotein E alleles